European Journal of Agronomy 105 (2019) 129–145

Contents lists available at ScienceDirect

European Journal of Agronomy

journal homepage: www.elsevier.com/locate/eja

A simple model simulating development and growth of an olive grove

M. Moriondo[a,*], L. Leolini[b], L. Brilli[a], C. Dibari[a,b], R. Tognetti[c], A. Giovannelli[d], B. Rapi[a], P. Battista[a], G. Caruso[e], R. Gucci[e], G. Argenti[b], A. Raschi[a], M. Centritto[d], C. Cantini[d], M. Bindi[b]

[a] IBIMET-CNR, Via G. Caproni 8, 50145 Firenze, Italy
[b] University of Florence, DAGRI, Piazzale delle Cascine 18, 50144 Firenze, Italy
[c] Dipartimento di Agricoltura, Ambiente e Alimenti, Università degli Studi del Molise, Via Francesco De Sanctis, 86100 Campobasso, Italy
[d] Trees and Timber Institute, National Research Council of Italy (IVALSA-CNR), Via Madonna del Piano 10, 50019 Sesto Fiorentino (Firenze), Italy
[e] Dipartimento di Scienze Agrarie, Alimentari e Agro-ambientali (DiSAAA-a), Università di Pisa, Via del Borghetto, 80 56124 Pisa, Italy

ARTICLE INFO

Keywords:
Olive trees
Model
Process-based
Transpiration
Yield

ABSTRACT

This paper describes the architecture of a process-based model that simulates on a daily time step growth and development of an olive agroecosystem, including the olive tree and grass cover growth and their competition for water. The key process of the model is the simulation of daily potential biomass increase for olive tree and grass cover that may be reduced depending on water availability. The model includes a phenological sub-model simulating the sequence of olive tree vegetative and reproductive stages for determining changes in biomass allocation and the timing of possible environmental stresses (heat and water stress) that may reduce final yield.

The model was calibrated and validated in Tuscany region by exploiting a data set covering heterogeneous climatic features as well as soil types and management practices existing in this region. The results pointed out that the model is able to faithfully reproduce water balance of the system, biomass accumulation and yield of olive tree and grass cover biomass. We concluded that this model is a useful prognostic tool to test the effectiveness of management practices for improving economic viability of olive tree cultivation.

1. Introduction

Olive orchards are widespread agricultural systems in the Mediterranean environments (Vossen, 2007), where they play a significant role for local economies (Iraldo et al., 2013; Palese et al., 2013) and contribute to several ecosystem services (Loumou and Giourga, 2003; Fleskens et al., 2008), including mitigation of carbon emission in the atmosphere (Nieto et al., 2010; Brilli et al., 2013, 2016, 2018; Nardino et al., 2013; Lorite et al., 2018). In particular, olive cultivation, having a limited water requirement, may exploit marginal areas characterised by shallow soil and sloping terrain that would be hardly used for other crops (Loumou and Giourga, 2003). The conservation of such agroecosystem is especially important for these areas, where the economic viability of olive tree cultivation is already threatened by highly fragmented private properties and the lack of appropriate management practices that result into high production cost and lower yield (Duarte et al., 2008).

In this context, crop-modelling approach is a useful tool that provides growers with reliable information on crop status during the season, which may help in decision-making process for the application of proper management practices. Further, these tools may help land managers to explore the suitability of olive tree cultivation in a future climate (Morales et al., 2016), where olive tree is expected to suffer higher temperatures and summer drought (Moriondo et al., 2008, 2013; Ferrise et al., 2013; Ponti et al., 2014; Brilli et al., 2018; Lorite et al., 2018).

In this paper, we present a new olive grove model, based on process-based algorithms, designed to simulate olive tree phenology, biomass accumulation and yield considering water competition with ground cover and the impact environmental stresses on yield. The model was developed bearing in mind that process-based models developed so far for olive tree require in many cases the calibration of multiple parameters and need many input variables to provide reliable results (e.g. López-Bernal et al., 2018; see the review in Moriondo et al., 2015 for a more comprehensive analysis of modelling approaches). These major requirements for input data and parameters make the approach not readily applicable on a local scale either for monitoring the current growing season or on a regional scale for planning strategies (Challinor et al., 2004; Soltani and Sinclair, 2011). The development of simplified models that require fewer input variables and parameters (e.g. Villalobos et al., 2006; Maselli et al., 2012; Lorite et al., 2018), would therefore a desirable target to extend the application of crop models to

* Corresponding author.
E-mail address: marco.moriondo@cnr.it (M. Moriondo).

https://doi.org/10.1016/j.eja.2019.02.002
Received 23 October 2018; Received in revised form 28 January 2019; Accepted 5 February 2019

areas where such a detailed information is missing. As drawback, the application of these models may be limited to the range of their calibration dataset (Monteith, 1996).

With these premises, we developed a model with a limited requirement for input data and parameters. The performances of the model were tested across sites having contrasting climates, soils, planting density and management practices, to ensure its applicability in conditions different from those of calibration area. The validation tests considered two strategies: i) the model was tested against data from experimental plots, where the variables requested to run the model and growth processes were locally measured; ii) the model was applied for assessing final yield on at farm scale, where input variables were available on a coarser resolution from spatial databases.

Aiming at provide a tool for optimizing crop management strategies (Fernández et al., 2008), the results are discussed emphasizing the compromise between the simple structure of the model and its effectiveness in reproducing different plant processes across different management practices and a gradient of Mediterranean climates.

2. Materials and methods

2.1. Model description

The model simulates growth and development of the olive agroecosystem on a daily time step, which includes the simulation of olive tree and grass cover growth and their competition for water (Fig. 1). A phenological sub-model simulates the sequence of olive tree vegetative and reproductive stages for determining changes in biomass allocation. Final yield is calculated at the end of growing season as a fraction of total olive tree biomass accumulation (harvest index, HI) that may be reduced from its potential value by both heat and water stress.

2.1.1. Olive tree phenology model

Bud break and flowering phases were simulated through two modelling approaches. Building on the results in López-Bernal et al. (2017), demonstrating olive tree apical buds undergo an easily-reversible dormant state in winter as driven by warm temperature, the onset of bud break is simulated considering forcing temperatures calculated as growing degree hours accumulation (GDH) above a base temperature (*tb*) from the 1st of January until a required accumulation (Eq. (1)).

$$GDH = \sum T_{avg(h)-tb} \quad (1)$$

where *GDH* is the growing degree hour accumulation above *tb* using hourly average temperature ($T_{avg(h)}$). The starts of dormancy state of the buds (i.e. the stop of the growing phase) is assumed to be triggered when average daily temperatures are stably below the *tb*.

Considering that the occurrence of flowering stage is dependent on both endogenous factors, regulating the release from endo-dormancy period, and exogenous factors, determining the release from eco-dormancy period (Sarvas, 1974), we adopted the UniChill model proposed by Chuine (2000). In this model, the duration of endo-dormancy period is dependent on chill units, calculated according to Eq. (2), that are cumulated from the end of summer until the chilling requirement is

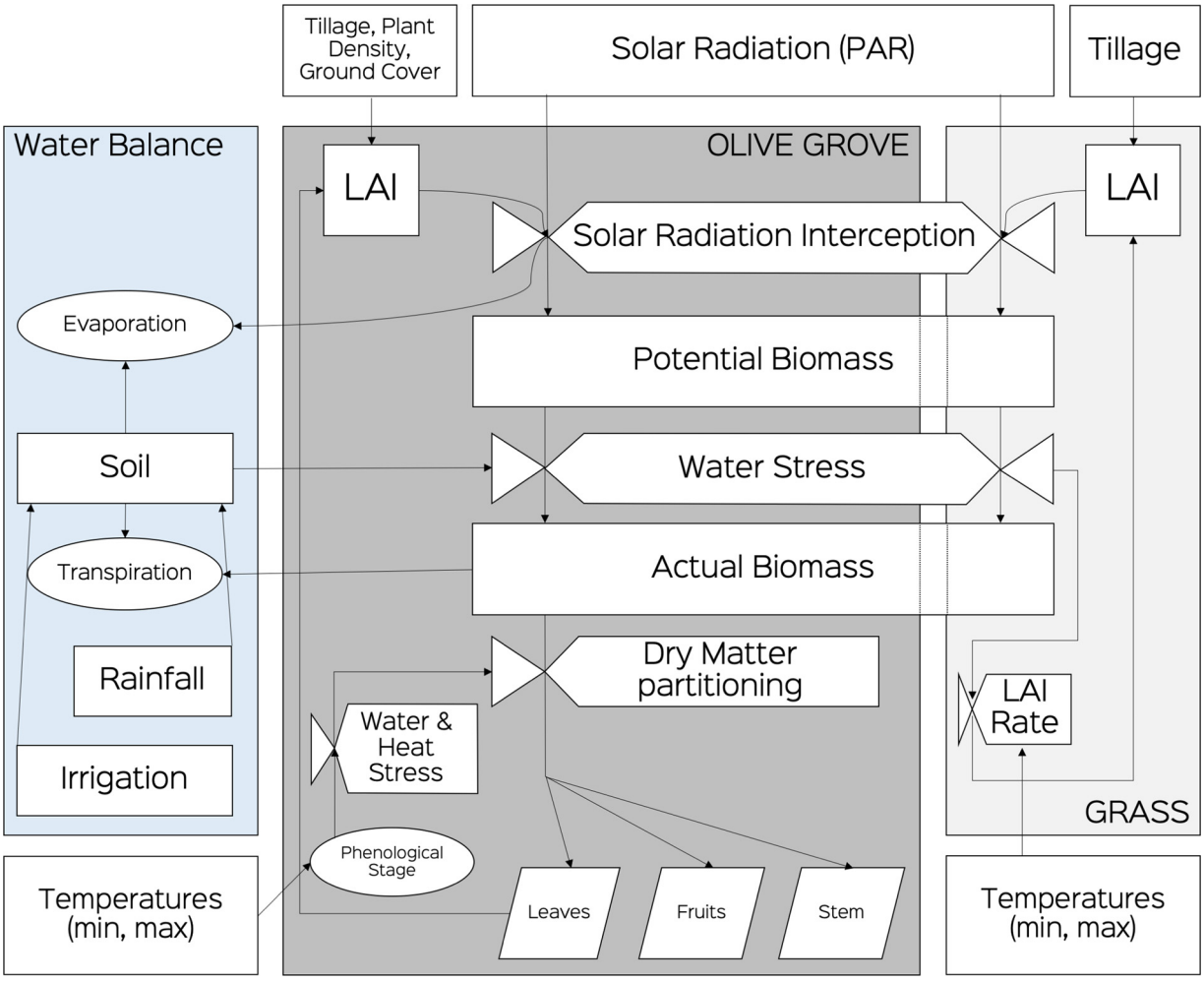

Fig. 1. Flow diagram of the model including the simulation of olive tree and grass cover growth and development.

reached (*Ccrit*). The duration of eco-dormancy period is dependent on forcing units, calculated according to Eq. (3), cumulated from the end of endo-dormancy to flowering stage (*FcritFlo*). September 1st was selected as initial date for chilling accumulation as in temperate zones chill temperatures do not occur before this time (Chuine et al., 1999).

Chilling and forcing units (CU and FU) are calculated as:

$$Chilling\ \ Units = \frac{1}{1 + e^{a\cdot(T_{avg}-c)^2+b\cdot(T_{avg}-c)}} \quad (2)$$

$$Forcing\ \ Units = \frac{1}{1 + e^{d\cdot(T_{avg}-e)}} \quad (3)$$

where T_{avg} is the daily average temperature, *a*, *b*, *c*, *d* and *e* are the curve shape parameters that define the rate of CU and FU in response to temperature.

2.1.2. Potential dry matter accumulation

A model was developed and tested to simulate daily biomass accumulation of an olive agroecosystem, which includes the simulation of olive tree (*ot*) and grass cover (*gr*) growth and their competition for water. The key process of the model is the simulation of daily potential biomass increase (dry matter [DM], g m^{-2}) for both layers as dependent on the relevant intercepted (*Int*, %) daily photosynthetic active radiation (*Rad*, MJ m^{-2}), and radiation use efficiency (*RUE*, g MJ^{-1}). Accordingly:

$$DM_i = Int_i \cdot Rad \cdot RUE_i \quad (4)$$

where the sub-index *i* refers to either olive trees (*ot*) or grass (*gr*).

Intercepted radiation of olive tree (Int_{OT}) was calculated according the model proposed by Testi et al. (2006) and applied in Villalobos et al. (2006):

$$Int_{OT} = 1 - \exp(1 - k' \cdot v) \quad (5)$$

where *v* is the canopy volume for unit area (m^3 m^{-2}) and *k′* is the extinction coefficient calculated as:

$$k' = 0.52 + 0.000788 \times PlantD - 0.76 \cdot \exp(-1.25 \times LAD) \quad (6)$$

where *LAD* is Leaf Area Density (m^2 m^{-3}) and *PlantD* is the number of plants per hectare.

At the beginning of the growing season, initial LAI of olive tree is calculated as:

$$LAI_{ini} = Vol \cdot LAD \cdot PlantA^{-1} \quad (7)$$

where *Vol* (m^3) is the volume of the crown of olive tree calculated as the volume of an ellipsoid and *PlantA* is plant spacing (i.e. inter-row × intra-row distances, m^2).

On each daily time step, the potential increase of olive tree LAI (LAI_{inc}) is calculated as the product of daily assimilated DM, a leaf partition coefficient (PC_{lf}, rate) and specific leaf area (*SLA*, m^2 g^{-1}). Accordingly:

$$LAI_{inc} = DM \cdot PC_{lf \cdot pot} \cdot SLA \quad (8)$$

PC_{lfpot} changes dynamically during the season depending on phenological stage accounting for the fact that before anthesis biomass is allocated only for vegetative biomass while after anthesis yield has highest priority for carbon allocation (Mariscal et al., 2000, details in Section 2.2.2). The effect of alternate bearing on source/sink relationships is also accounted for by considering that in over-cropping years vegetative growth is reduced and *vice versa* (Lavee, 2007) (Section 2.1.4 for details).

Cumulated LAI is then used to update the canopy volume for unit area (*v*) daily as used in Eq. (5) and calculated as:

$$v = LAI \cdot LAD^{-1} \quad (9)$$

Considering that the typical life span of olive tree leaves is two-year (Morales et al., 2016), leaves senescence is calculated as:

$$Sen_{leaf} = \frac{YLAI_{(y-2)}}{DOY_{end} - DOY_{ini}} \quad (10)$$

where *YLAI* is the LAI produced two years before and DOY_{end} and DOY_{ini} are the days when senescence ends and begins, assumed between DOY 365 and 1 (Morales et al., 2016).

Total dry matter cumulated from January 1st to harvest time is converted into final yield, using a fixed ratio between final yield (*Y*) and total dry matter (potential harvest index, *HI.pot*, %). Accordingly:

$$Y = HI.\ pot \times \sum_{DOY=1}^{DOY=harvest\ \ time} DM \quad (11)$$

In unstressed conditions *HI.pot* has an initial value of 0.35 (Villalobos et al., 2006) that may be decreased by unfavorable meteorological events occurring at flowering and fruit set or affected by alternate bearing (see Section 2.1.4 for details).

The fraction of radiation penetrating olive tree canopy (1 − Int_{ot}, %) is available for grass growth and the relevant intercepted radiation is calculated as:

$$Int_{GR} = 1 - \exp(-k \cdot LAI) \cdot (1 - Int_{OT}) \quad (12)$$

where *k* is the extinction coefficient and LAI is grass cover leaf area index.

LAI growth for grass was modelled according to the approach proposed by Celette et al. (2010) for simulating water balance of an intercropped vineyard (WaLIS model). Accordingly, daily potential LAI increase of grass cover (*LAIgr*) is calculated as the difference between the daily LAI increase (*GLAId*) and daily LAI senescence (*SLAId*):

$$LAI_{gr} = GLAI_d - SLAI_d \quad (13)$$

In not stressed conditions, *GLAId* is dependent on LAI growth rate of grass cover (*LAI-rate*, m^2 m^{-2} day^{-1}) and *Ft* (unit less) that is calculated as a quadratic function of temperature, ranging between 0 (at 0 °C) and 1 (at 18 °C):

$$GLAI_d = LAI_{rate} \cdot Ft \quad (14)$$

The fraction of LAI produced each day ($GLAI_d$) is initialized with zero degree-days, and the thermal time during the life of this fraction is calculated daily as DDA included between 0 and 18 °C. When the cumulated thermal time of any given fraction of LAI reaches the thermal time threshold set by the leaf duration crop input parameter (700 °C DDA), this fraction is assumed to be senescent and it is subtracted from the total LAI.

Under not limiting moisture conditions, DM calculated for both olive tree and grass cover is converted into relevant transpired water (Tr_{OT}, Tr_{GR}, mm m^{-2} d^{-1}), according to the relationship between biomass production and crop transpiration (Tanner and Sinclair, 1983; Sinclair et al., 1984): Accordingly:

$$Tr_i = DM_i \cdot TE_i^{-1} \quad (15)$$

where *Tr* is daily crop transpiration and *TE* is transpiration efficiency defined by:

$$TE_i = \frac{Kd_i}{VPD} \quad (16)$$

where *VPD* is daily water pressure deficit (kPa) and *Kd* (Pa) is a species dependent coefficient (transpiration efficiency coefficient).

Considering that in Eq. (16) *VPD* is in kPa and *Kd* is in Pa, the conversion of biomass into transpiration unit results from g m^{-2} day^{-1} to kg (or mm) day^{-1}. The sub-index *i* refer to either olive trees (*ot*) or grass (*gr*).

2.1.3. Water balance and impact of water stress on potential growth

In order to consider the specific characteristics of a typical olive grove, which includes olive trees and grass cover, we defined a simplified soil system with two different overlaid soil layers as delimited by

root system depth of these plants. The first is between soil surface and root depth of grasses, the second between root depth of grasses and maximum depth of olive tree roots.

Each layer is defined by its water content availability (*WCA*, i.e., the water included between field capacity and wilting point [$m^3\,m^{-3}$]) and total transpirable soil water (*TTSW*, mm) (i.e., *WCA* × layer depth [mm]).

Accordingly, total transpirable soil water over the entire profile:

$$TTSW = TTSW_1 + TTSW_2 \quad (17)$$

Soil water balance is tracked for each layer of the soil profile. A cascade model interconnects the two layers so that, if the amount of water entering the first layer exceeds its field capacity, the remaining water enters the layer below. Assuming no surface runoff, available soil water for each layer (*ATSW*, mm) depends on its value from the previous day as refilled by precipitation (Rain, mm) or irrigation (*Ir*, mm), and depleted by evaporation from soil surface (*SEVP*, mm) and olive tree and grass transpiration (Tr_{OT}, Tr_{GR}). Given that grasses and olive tree root systems explore different soil depths and compete for water only in layer 1, *ATSW* in this layer was calculated on a day *d* as:

$$ATSW_1 = ATSW_{1(d-1)} + Rain + Ir \quad (18)$$

If the ATSW1 exceeds TTSW1, then the excess water enters layer 2. Accordingly:

$$ATSW_2 = ATSW_{2(d-1)} + (ATSW_1 - TTSW_1) \quad (19)$$

On the evidence that a stable response function exists between plant gas exchange and extractable soil water content (Sinclair et al., 1998), we used the ratio between the actual water content *ATSW* and *TTSW* (i.e., fraction of transpirable soil water, *FTSW*) as index to rescale potential transpiration for olive trees and grass cover to its actual value. Similarly, a stable response function exists between leaf area development and soil water content (Bindi et al., 2005), and the same FTSW can be used to rescale leaf area growth from its potential value.

FTSW for layer 1 is calculated as:

$$FTSW_1 = \frac{ATSW_1}{TTSW_1} \quad (20)$$

while *FTSW* over the entire profile (layer 1 + layer 2) is calculated as:

$$FTSW_{1\_2} = \frac{ATSW_1 + ATSW_2}{TTSW_1 + TTSW_2} \quad (21)$$

FTSW affects transpiration and leaf area growth of both olive tree and grass cover according to the general equation as proposed in Sinclair (1986) and Bindi et al. (2005) (SI_1):

$$RelTr\,(RelLAI) = \frac{1}{1 + a \cdot e^{(-b \cdot FTSW)}} \quad (22)$$

where *RelTr (RelLAI)* is the fraction of actual to potential transpiration (leaf area growth) and ranges from 1, when *FTSW* is not yet limiting potential transpiration (leaf area growth), to 0 where FTSW completely inhibits transpiration (leaf area growth) and *a* and *b* are empirical parameters shaping the response of *RelTr* and *RedLAI* to *FTSW*. *RelTr* and *RedLAI* are dependent on $FTSW_{1\_2}$ for olive tree and on $FTSW_1$ for grass cover.

Accordingly, transpiration of olive tree and grass cover are rescaled from the relevant potential value *Tr* defined in Eq. (15) to their actual value *ATr* ($mm\,m^{-2}\,d^{-1}$):

$$ATr_i = Tr_i \cdot Re\,lTr_i \quad (23)$$

The same approach is used to reduce potential leaf area growth of olive tree (LAI_{inc}) and grass cover (*GLAId*). When soil water is not able to sustain leaf area growth at its potential rate, LAI_{inc} of olive tree is rescaled to its actual value ($ALAI_{inc}$) using the relationship between *FTSW* and leaf area growth (*RelLAI*):

$$ALAI_{inc} = LAI_{inc} \cdot Re\,lLAI_{ot} \quad (24)$$

For grass cover, *GLAId* is rescaled to its actual value ($AGLAI_d$) according to:

$$AGLAI_d = GLAI_d \cdot WIC \quad (25)$$

$$WIC = \max\left(0, \min\left(1, \frac{FTSW_1}{FTSW_{thrLAI}}\right)\right) \quad (26)$$

where $FTSW_{thrLAI}$ is water stress threshold for reducing growth of leaf area.

For olive tree, the model accounts for the increase in TE in response to water stress conditions (Villalobos et al., 2012). A linear function was applied to modify *TE* when stomatal opening starts to be affected by water stress (Fig. 5 in SI_2). This function was calibrated using the experimental data reported in Villalobos et al. (2012) by considering the relative increase in transpiration efficiency (*RelTE*) as function of *RelTr*:

$$RelTE = -0.74 \cdot RelTr + 1.74 \quad (27)$$

Because of reduced transpiration and increased *TE*, DM of olive tree is rescaled to its actual value (*ADM*):

$$ADM_{ot} = DM_{ot} \cdot RelTr_{ot} \cdot RelTE \quad (28)$$

For grass cover, we considered a fixed TE and therefore actual dry matter is calculated as:

$$ADM_{gr} = DM_{gr} \cdot RelTr_{gr} \quad (29)$$

Finally, at the end of day *n*, $ATSW_1$ and $ATSW_2$ are updated considering olive tree and grass cover transpiration and soil evaporation SEVP.

$$ATSW_1 = ATSW_1 - [ATr_{GR} + (ATr_{OT} \cdot sf1) + SVEP] \quad (30)$$

$$ATSW_2 = ATSW_2 - (ATr_{OT} \cdot sf2) \quad (31)$$

where *sf*1 and *sf*2 are scalar factors to account for olive tree transpiration over the entire soil profile that is proportionally partitioned between layer 1 (*sf*1 = thickness of layer 1/maximum rooting depth) and layer 2 (*sf*2 = thickness of layer 2/maximum rooting depth).

Potential *SEVP* is calculated as evaporation from a wet soil surface using a simplified Penman equation (Soltani and Sinclair, 2012), where driving variables are vapor pressure curve versus mean temperature (*DELT*), incident daily solar radiation (*SRAD*), and soil albedo (*SALB*). *SRAD* is discounted to account for the interception of radiation by the plants canopy (olive tree + grass). This potential value is calculated for a rainfall event greater than 10 mm. If FTSW over the entire profile is lower than 0.5, potential *SEVP* is rescaled as a function of the square root of time since the start of the dry spell (*DYSE*, number of days) (Soltani and Sinclair, 2012).

$$SEVPpot = SRAD \times (1 - SALB) \times (1 - INT.tot) \times \frac{DELT}{DELT + 0.68} \quad (32)$$

$$DELT = EXP\left(\frac{21.255 - 5304}{273 + TMP}\right) \times \left(\frac{5304}{((273 + TMP)2)}\right) \quad (33)$$

$$SEVP = SEVP \times [(DYSE + 1)^{1/2} - DYSE^{1/2})] \quad (34)$$

2.1.4. Simulation of environmental stresses, harvest index and alternate bearing

The model considers both water and heat stresses occurring at anthesis as reducing factors of HI.pot using a linear function that describes the decrease of yield as dependent on the intensity of these events.

The results of Moriana et al. (2003) and Rapoport et al. (2012) were used to identify the cardinal values of this function for water stress, corresponding to FTSW below which water stress starts to affect final yield (*FTSWo*), and FTSW corresponding to yield = 0 (*FTSWm*).

Following the results reported in these papers, the average FTSW calculated at anthesis ($FTSW_{ant}$) was used to linearly rescale HI.pot

from its unstressed value (0.35) to its actual value (*HIws*) when $FTSW_{ant} < FTSWo$:

$$HIws = HI.pot \times \left(1 - \frac{(FTSWo - FTSWant)}{FTSWo - FTSWm}\right) \quad (35)$$

where *FTSWo* is 0.4 and *FTSWm* corresponding to *HIws* = 0 (Fig. 6 in SI_2).

A similar approach was used to account for the impact of maximum temperatures at anthesis that were reported to affect pollination and fruit set for values higher than 30 °C (*TMAXo*) (Rapoport, 2014; Benlloch-González et al., 2018). Accordingly, in the model, average Tmax around anthesis ($TMAX_{ant}$) was used to decrease linearly HI from its potential value to its actual value for $TMAX_{ant} > 30$ °C. The results from Koubouris et al. (2009) were used to parametrize the maximum temperature corresponding to HI = 0 ($TMax_m = 40$ °C). Accordingly, when $TMax_{ant} > TMax_o$.

$$HIhs = HI.pot \times \left(1 - \frac{(TMAXant - TMAXo)}{(TMAXm - TMAXo)}\right) \quad (36)$$

Finally, the actual HI (*HIa*) is calculated by considering as additive the effect of *HIws* and *HIhs*.

The model simulates alternate bearing, where a poor fruiting occurring on a year *n* results into over-cropping and reduced vegetative growth during the year *n* + 1 (Lavee, 2007). To account for this effect, we introduced in the model a function to account for increased production in the year *n* + 1 following a reduced production (*HIa* < 0.35) in year *n*. Accordingly the new *HI.pot* is increased by:

$$HI.pot = 0.35 + (0.35 - HIa) \quad (37)$$

While to account for reduced vegetative growth, partition coefficient to leaves (PC_{lf}) is decreased by:

$$PClf = PClf.pot \times [1 - (0.35 - HIa)] \quad (38)$$

The new *HI.pot* may be subjected the same to stress at anthesis in the following year according to Eqs. (35) and (36).

To account for the continuation of biannual trend on olive yield and vegetative biomass over a period, when *HIa* > 0.35 :

$$HI.pot = 0.35 - (HIa - 0.35) \quad (39)$$

$$PClf = PClf.pot \times [1 + (HIa - 0.35)] \quad (40)$$

According to the structure of the model, heat and water stresses at anthesis, unbalancing vegetative growth and fruit production, may trigger the beginning of alternate bearing or modify the current trend. These sub models, and their interaction, were tested over sites 6–12 that recorded a longer series of yield data providing a better benchmark to assess the alternate bearing trend. Yield records for each site were previously inspected to assess the degree of alternate bearing using Alternate Bearing Index (Pearce and Dobersek-Urbanc, 1967), calculated as follows:

$$ABI = \frac{1}{n-1}\sum_{i=1}^{n-1}\left(\frac{|Y_i - Y_{i+1}|}{Y_i + Y_{i+1}}\right) \quad (41)$$

where *Yi* is olive fruit yield of year i and n is the number of years considered. *ABI* = 0 corresponds to no alternate bearing while 1 corresponds to total alternate bearing. Assuming ABI > 0.3 as a threshold to define an alternate bearing trend, for each site above this threshold, in the first year of simulation, we set an *HIa* so that simulated final yield on that year matches relevant observed yield. After that, the model keeps on simulating yield considering the alternate bearing trend induced on the first year of the time series, where the additional impact of stresses at anthesis may reduce or enhance this trend. As an example, the implementation of this model on final yield is shown for a case study in Fig. 7 in SI_2.

2.2. Model calibration and validation strategy

2.2.1. Phenology model

GDH requirement for bud break and the relevant *tb* were calibrated using the average bud break dates recorded in two sites having a contrasting climate. Specifically, Follonica (warm site, 2007–2010, site C in Table 1 and Fig. 1 of SI_2) and Montepaldi (Mancuso et al., 2002) (cold site, 1996–1999, site B in Table 1 and Fig. 1 of SI_2) were selected since they exhibit a relative advance (DOY 80) and delay (DOY 103) in the occurrence of the stage. Since bud-break dates were available for both sites as an average value over the relevant study period, the meteorological dataset for calibration was obtained using an average year that was calculated by averaging, day by day, the daily minimum and maximum temperature over the period of observation (Montepaldi: 1996–1999, Follonica: 2007–2010). *tb* for GDH accumulation was calculated as the threshold providing the lowest difference in GDH amount calculated form 1st of January to observed dates of the stage in the sites.

The model for flowering was calibrated on four different sites, Florence (1993–2008), Prato (1992–1998), Lido di Camaiore (2001–2017) and Grosseto (2013–2017) (sites A, D, F, E in Table 1 of SI_2), using diagrams of olive tree aerial pollen concentration as proxy of the event (e.g. Moriondo et al., 2001; Orlandi et al., 2013). The pollen diagrams were previously inspected to detect possible interferences from other cultivated areas, which may lead to uncertainties in the identification of the anthesis stage. In general, the pollen concentration diagrams exhibited for all sites a single pollination period along the season that lasts in average 7 days with a clear peak of concentration. This made easy the identification of the anthesis occurrence recorded as the day of peak event.

Considering that in Tuscany Moraiolo and Frantoio represents more than 70% of varieties generally grown in the region (Cantini et al., 1999), we assumed these varieties as representative for all sites. Owing the fact that the anthesis of these varieties shows a good synchronicity (Mancuso et al., 2002), these were considered as a single variety and the datasets relevant to each site were therefore pooled together for calibration and validation.

Specifically, the optimization of parameters of Unichill model (*a*, *b*, *c*, *d*, *e* in Eqs. (2) and (3)) was performed by using the simulated annealing algorithm (Metropolis et al., 1953) implemented in Phenology Modelling Platform (PMP) version 5.5 (www.cefe.cnrs.fr). The dataset was previously split into a training set for the calibration, accounting for 80% of available data, while the remaining 20% of data were used for validation. The model parameters were fitted in a range as indicated in PMP program. Specifically, *a* varied in the range from 10^{-4} to 10, *b* from -30 to 15, *c* from −30 to 30, *d* from −40 to 0 and *e* from −30 to 30.

2.2.2. Growth model

The literature was surveyed and used to parametrize the growth model. RUE in not limiting water conditions for olive trees was obtained by Villalobos et al. (2012) (0.98 g dry matter MJ^{-1}). The relationships between FTSW and olive tree transpiration and leaf area (Eq. (22)) were obtained from a specific experiment conducted on pot-grown olive trees (see SI_1). Specifically, for olive tree, *a* = 6.17 and *b* = 13.45 for *RelTr* and *a* = 78.24 and *b* = 21.42 for *RelLAI*.

RUE of grass cover, which is represented by a typical forage mixture of species including grasses and legumes (Argenti et al., 2012), was set to 2.2 g MJ (Bélanger et al., 1992; Duru et al., 1995; Soltani and Sinclair, 2012). For grass cover, *a* and *b* parameters for RelTr were obtained from Schoppach and Sadok (2012) by assuming grass cover behaving like wheat crop to water stress. Owing to the fact that natural grass vegetation is highly adapted to the Mediterranean environment, we selected the most tolerant variety as representative of the drought-adapted natural grasses in the grove. Specifically, in Eq. (21), *a* = 15.17 and *b* = 11.45 for *RelTr*, the same parameters were assumed for *RelLAI*.

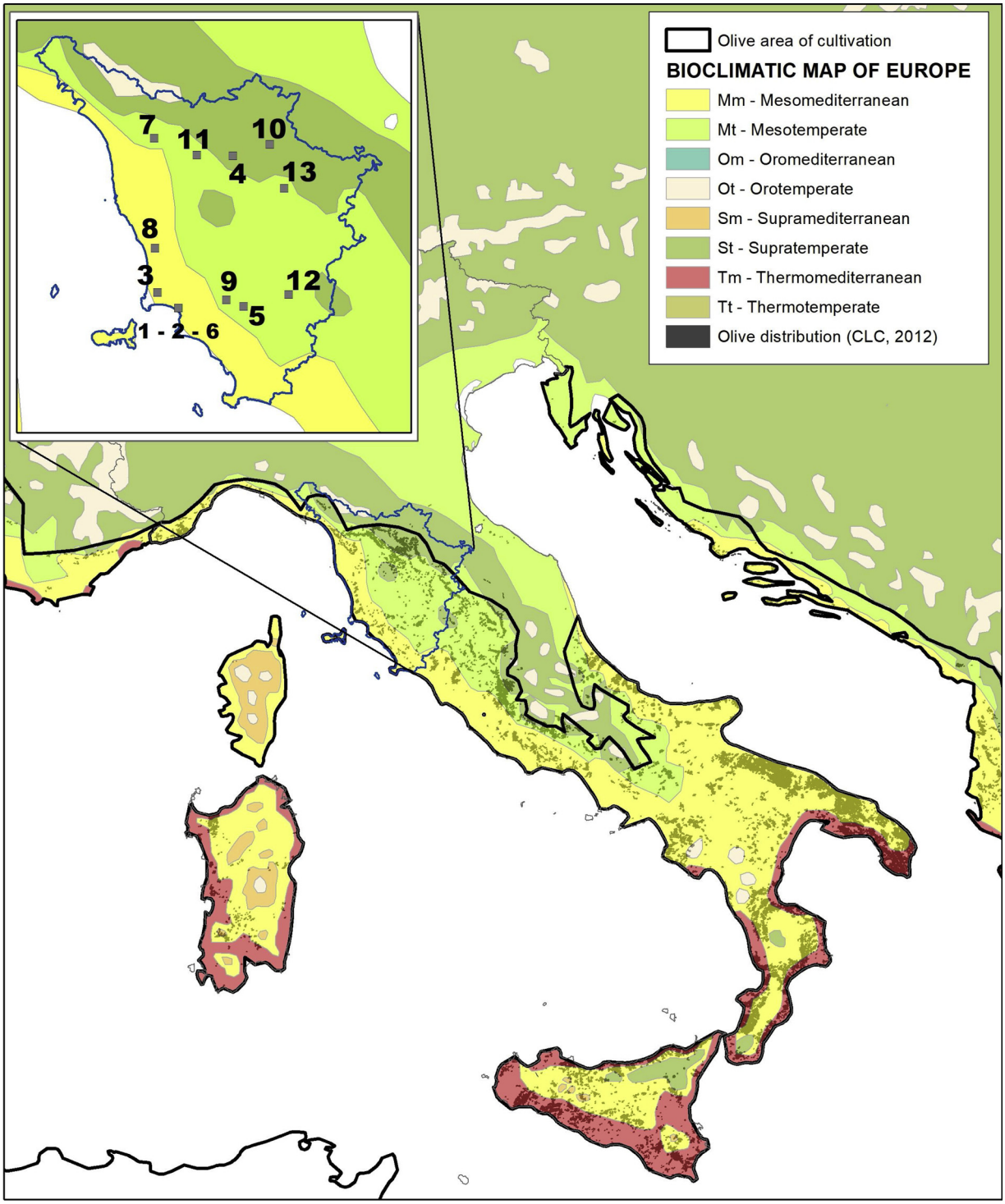

Fig. 2. Experimental sites distribution in Tuscany region and bio-climate classification of olive tree cultivated area in Italy. The bio-climate map is a modified from Rivas-Martınez et al. (2004), olive grove distribution and the limits of olive tree cultivation were obtained from Corine Land Cover and Moriondo et al. (2008).

Dry matter partitioning coefficients to leaves (PClf.pot) in olive trees before anthesis was set to 25% of daily assimilation (Mariscal et al., 2000), while after anthesis it was reduced to 9% to account for the lowest priority in carbon allocation (Morales et al., 2016). The potential proportion of final yield to total dry matter (potential harvest index, HI.pot) was obtained by Villalobos et al. (2006) for not-limiting water conditions (0.35). These coefficients were rescaled from the reported values in consideration that partitioning to roots, which was not included in the original measurements, accounts for 30% of total produced biomass (Nardino et al., 2013). Specific leaf area was set at $0.0042\,m^2\,g^{-1}$ (Villalobos et al., 2006).

Three parameters were calibrated, namely *Kd* for olive trees and grass and LAI-rate for grass using olive grove NPP measured in site 1 (Fig. 2, Table 1); in this olive grove, fluxes of carbon dioxide (CO_2), water vapor (H_2O), sensible heat (H) and latent heat (LE) between the biosphere and the atmosphere where monitored from 2010 to 2012. Gap-filling and flux partitioning were applied according to the Reichstein et al. (2005) procedure, providing a continuous record of net ecosystem exchange (NEE, $g\,C\,m^{-2}\,d^{-1}$), gross primary production (GPP, $g\,C\,m^{-2}\,d^{-1}$) and ecosystem respiration (Reco, $g\,C\,m^{-2}\,d^{-1}$).

Table 1
Sites description.

ID	Name	Experimental period	Lat N Lon E (°)	Elevation (m asl)	Varieties	Area (ha)	Plant spacing (m)	Ground cover (%)	Soil AWC (%)	Soil depth (m)	T_{avg} (°C)	T_{xHM} (°C)	T_{nCM} (°C)	*PP* (mm)	Clim
1	S. Paolina (CNR)	2010–2012	42.93–10.77	10	L, F, M	6	7 × 5	25	17	1.1	15.45	29.54	4.18	614	Mm
2	S. Paolina (CNR)	2012–2013	42.93–10.77	10	L	0.1	4 × 4	33	17	1.1	15.46	30.40	4.61	695	Mm
3	Venturina (UNIPI)	2008–2010	43.02–10.61	10	F	0.5	4.3 × 4.3	37	11	1.5	15.08	29.25	3.65	1016	Mm
4	Florence (ITAS)	2016	43.78–11.22	80	F	0.5	7 × 5	38	16	1	15.94	34.14	2.8	964	St
5	Paganico	1993	42.93–11.27	340	Tr, Fe, Lo	*	*	*	11	1	14.67	28.67	2.72	846	Mt
6	Follonica	1970–1986	42.93–10.77	10	L, F, M	1.5	7 × 5	20	16	1.1	15.35	29.07	3.80	631	Mt
7	Capannori	2002–2006	43.89–10.61	75	L, F, M	1.2	7 × 5	24	17[a]	1.4[a]	14.46	30.47	0.77	1067	St
8	Bibbona	1998–2006	43.27–10.60	25	L, F, M	2.3	7 × 5	23	12[a]	1.4[a]	15.43	29.88	3.51	530	Mn
9	Roccastrada	1998–2006	42.97–11.14	23	L, F, M	2.2	5 × 5	28	16[a]	1.1[a]	15.51	33.68	2.38	745	Mt
10	Londa	2001–2006	43.84–11.51	250	L, F, M	1.6	7 × 5	22	15[a]	0.79[a]	14.17	31.31	0.76	948	St
11	Vinci	1998–2006	43.79–10.94	260	L, F, M	1.5	7 × 7	24	11[a]	0.76[a]	14.18	29.71	1.92	832	Mt
12	Castiglione D'Orcia	1999–2006	42.99–11.62	350	L, F, M	1.2	7 × 5	19	15[a]	0.73[a]	13.67	28.89	1.4	662	Mt
13	Loro Ciuffenna	1999–2006	43.59–11.61	600	L, F, M	0.8	7 × 7	20	11[a]	0.76[a]	13.39	30.41	0.16	835	Mt

Varieties: L = var. Leccino, F = var. Frantoio, M = var. Moraiolo; Tr = subclover, Fe = tall fescue, Lo = ryegrass; * not applicable; T_{avg} = average yearly temperature, T_{xHM} = average maximum temperature of warmest month; T_{nCM} = average minimum temperature of the coldest month; PP = average yearly cumulated rainfall; Clim = climatic classification according to Rivas-Martinez et al. (2004) where Mn = Meso-Mediterranean, St = Supra-temperate, Mt = Meso-temperate.

[a] Soil data were extracted from the regional database described in Gardin and Vinci (2006) reporting soil texture and depth. Soil texture was converted into soil AWC using pedo-transfer function (Saxton et al., 1986).

GPP was firstly transformed in dry matter considering the carbon/dry matter ratio (0.49), which was then converted in net primary production (NPP) using a fixed NPP/GPP ratio (0.4). This value was derived from observed data obtained by Nardino et al. (2013) in an olive grove (~0.4) that is in accordance to the value obtained for shrubs evergreen in Zhang et al. (2008).

The calibration was performed in 2010 by minimizing the root mean square error (RMSE) between NPP observed and simulated in 2010. *Kd* for olive trees and grass were iteratively tested in a range from 3 to 10 Pa (step 0.25) and LAI-rate for grass in a range from 0 to 0.1 (step 0.05). For each iteration, daily-simulated NPP, cumulated per ten days, was compared to relevant observed data and the coefficients minimizing the RMSE were selected.

The calibrated model was then applied to simulate NPP in 2011 and 2012 in the same site (see SI_MAT_MET for details).

The calibrated model was further tested to assess its performances in simulating specific processes of olive tree, grass cover growth and final yield. In site 2 and site 4 (Fig. 2, Table 1), the model was tested in simulating soil water dynamics and transpiration. In site 3 (Fig. 2, Table 1), the model was tested in simulating LAI increase, total olive tree biomass accumulation and final yield of olive trees under different irrigation treatments (full irrigation, 50% deficit irrigation and complementary irrigation) from 2008 to 2010. In the same site, the model was tested in 2012 for total olive tree biomass accumulation, final yield and grass cover total biomass using the data reported in Scandellari et al. (2016). In site 5 (Fig. 2, Table 1), the grass cover model was tested against daily growth rate of a typical Mediterranean mixed grass in 1994. In sites 6–13 the model was applied to simulate final yield on a farm level, in areas showing different elevations, climate, soils and planting density (Fig. 2, Table 1). Additional description of the sites and further details of the experiments may be found SI_MAT_MET.

Root mean square error (RMSE, Eq. (1) in SI_MAT_MET), Relative Root Mean Square Error (RRMSE, Eq. (2) in SI_MAT_MET), correlation coefficient *r*, Mean Bias and Absolute errors (MBE, MAE Eqs. (3) and (4) in SI_MAT_MET) were used as goodness of fit indicators.

We used Latin hypercube sample (LHS) method to explore the behavior of the model in response to a specific variation of its parameters or input values, using 1999 at site 1 as test case, considered as an average year of the area. Specifically, LHS is a regression approach that measures how strong the linear association is between the model output and each input parameter, while controlling the effect of the other factors (partial rank correlation coefficient, PRCC) (Confalonieri et al., 2010).

We tested the model sensitivity in terms of total yearly cumulated biomass of grass and olive trees to changes in physiological parameters (RUE, Kd, LAI rate, RelTE), a and b coefficients shaping the response of olive transpiration and leaf area growth to water stress, grove architecture (inter-row and intra-row distances and crown dimensions), soil parameters (root depth and AWC). Assuming that the default value of each parameter is the average of a population normally distributed, the value of each parameter was tested over the relevant population as defined by a fixed standard deviation (10% of default value).

The results are shown in terms of *PRCC* between a parameter or variable and the total biomass accumulation of olive tree and grass cover.

3. Results

3.1. Phenology model

The calibration of bud break model evidenced that the advancement in the occurrence of the stage in the warmer site (Follonica) with respect to the cooler one (Montepaldi) (23 days) was well simulated cumulating 3420 GDH from 1st of January with $tb = 8.5$ °C.

The Unichill model calibrated for flowering well simulated differences in the occurrence of this stage between sites, where Grosseto

showed a general advance of anthesis (average observed DOY = 147 versus average simulated DOY = 147) with respect to Lido (152 versus 151), Florence (152 versus 152) and Prato (156 versus 155). The model further accounts for a good simulation of the inter-annual variability with an RMSE = 3dd and RRMSE = 15% yielded in the calibration dataset and RMSE = 3.8dd RRMSE = 22% in the validation (Fig. 2 in SI_2).

The model calibration evidenced that 185 CU are requested to fulfill chill requirements for endo-dormancy period (*Ccrit*), where CU are cumulated for daily average temperatures lower than 9 °C. The cumulated forcing units requested for anthesis (*FcritFlo*) were 80 FU, where FU are effective for average temperatures higher than 8.5 °C.

3.2. Growth model

According to the optimization procedure, LAI-rate, *Kd* for olive trees and grass were set to the values minimizing the relevant RMSE, which corresponded to 0.025 d^{-1}, 6.5 Pa and 5 Pa (Fig. 4 SI_2). Under this configuration, the relationship between observed and simulated data in 2010, cumulated per ten-days, yielded a RMSE = 7.6 g m^{-2} with an RRMSE = 17% and r = 0.81 (Table 3). On a yearly basis, the model underestimated cumulated olive grove biomass (751 g m^{-2}) with respect to what observed (818 g m^{-2}).

The calibrated version of the model faithfully reproduced the seasonal trend of NPP when applied in the same grove in 2011 and 2012 (Fig. 3b and c). In particular, the model satisfactorily simulated NPP in the validation datasets by detecting the effect of prolonged drought periods that occurred in both years, which reduced the observed assimilation rate of the grove with respect to 2010. Cumulated rainfall in 2011 and 2012, in fact, was 54% and 71% with respect to 2010 (697 mm), in the period included between January 1st and the harvest date (DOY 330). The lower rainfall, especially during the soil water recharge period (winter), resulted in a reduced biomass accumulation observed in both years with respect to 2010 with a total cumulated NPP of 642 in 2011 and 583 g m^{-2} in 2012. The model correctly simulated this trend, with a very good performance. In 2011, on a ten-days basis, the correlation between simulated and observed data yielded an r = 0.85 with an RMSE = 6.8 g m^{-2} and RRMSE = 23%. On a yearly basis, the simulated olive grove cumulated NPP (709 g m^{-2}) was slightly overestimated with respect to the observed one (642 g m^{-2}).

In 2012, the daily trend of NPP was well captured by the model (Fig. 3c), with two main peaks detected in early and late spring, were the output of the simulation over the season resulted as overestimated (649 g m^{-2}) with respect to observed data (583 g m^{-2}). On a ten-day basis the performances were in line with results of previous years, with an r = 0.82, RMSE = 5.6 g m^{-2} and RRMSE = 17% (Table 3).

The calibrated model was further tested to evaluate its performances in simulating olive tree transpiration, water balance, grass cover and olive tree biomass accumulation and final yield.

The model faithfully simulated the seasonal trend of transpiration rate in site 2 in 2012 and 2013 (Fig. 4). The model correctly simulated the depressing effect of drought stress at the end of the growing season in 2012, the increasing trend of transpiration observed in 2013 at the start of growing season due to abundant rainfall (from DOY 100 to 122), and the progressive effect of drought in summer. It should be noticed that the model in some cases tends to underestimate periods with a lower evaporative demand as those occurring during consecutive rainy days (from DOY 121 to 151). On a daily basis, the simulation yielded correlation coefficient of 0.86 with an RMSE of 0.43 mm and RRMSE = 15% (Table 3). The good results in the simulation of transpiration was associated to the satisfactory simulation of the daily course of FTSW in the same site in 2013, in the top layer (0–30 cm, r = 0.94, RMSE = 7.7%, RRMSE = 7.7%) and over the entire soil layer explored by roots (r = 0.95, RMSE = 11%, RRMSE = 11%) (Table 3) (Fig. 5a and b).

Similar performances were observed in site 4 (Fig. 6a and b), where FTSW was satisfactory simulated with an underestimation over the top layer (r = 0.91, RMSE = 10%, RRMSE = 10%) and a slight overestimation when considering the entire soil profile (r = 0.94, RMSE = 6.5%, RRMSE = 6.5%) (Table 3).

The results indicated the overall good performances of the model in simulating total olive tree biomass accumulation, yield and LAI in site 3 under three different irrigation treatments (2008, 2009, 2010 and 2012) (Fig. 7a–c). Overall, when pooling together the outputs for site 1 and site 3 (Fig. 7a and b), the simulation of biomass accumulation yielded r = 0.92, RMSE = 1.2 Mg ha^{-1} and RRMSE = 10%, while final yield resulted in r = 0.95, RMSE = 0.58 Mg ha^{-1} and RRMSE = 11% (Table 3). The model correctly detected the yearly LAI increments recorded over the period 2008–2010 in site 3 with r = 0.9, RMSE = 0.07 and RRMSE = 17%, (Fig. 7c, Table 3).

When applied over farm sites, the model, accounting for the effect of alternate bearing and environmental stresses at anthesis, satisfactorily simulated inter annual yield variability (Fig. 7d), showing r = 0.77 and RMSE = 0.41 Mg DM ha^{-1} and RRMSE = 18% (Table 3).

In site 5, the grass cover model captured the observed trend of grass growth rate with a main peak in early spring, and a secondary one in autumn, even though in advance with respect to observed data (Fig. 8). Overall, the model provided good performances in terms of r (0.96), RMSE (5.6 kg ha^{-1} day^{-1}) and RRMSE (11%). Further, in site 3 the model correctly simulated the biomass partitioning between olive and grass biomass in 2012, where yearly grass cover growth yielded 25% of total olive grove NPP versus 28% really observed in the field (Nardino et al., 2013).

3.3. Sensitivity analysis

The PRCC obtained via LHS indicated that in the model olive and grass biomass accumulation is highly sensitive to the relevant intercepted radiation and RUE parameters (Fig. 9). Olive dimensions (radius) ranked the first in PRCC analysis for the accumulation of olive tree biomass (Fig. 9a), showing the highest degree of association with olive tree biomass (0.9). Olive tree spacing follows (inter-row and intra-row) with a negative correlation (−0.84) and RUE with 0.79. LAI growth rate ranked the first for grass growth (0.94), followed by grass RUE (0.81) (Fig. 9b).

PRCC analysis highlighted that there is a clear interaction between the considered agro-ecosystem elements. Decrease in plant spacing of olive tree and larger crown dimensions, while increase biomass accumulation of olive tree, reduce the accumulation of grass cover due to the effect of increasing shading by trees as shown by a negative PRCC between grass growth and radius (−0.62) and a positive one with inter-row (0.61) and intra-row (0.45) (Fig. 9b). On the other hand, LAI rate that is the parameter most influencing grass biomass accumulation showed a negative, though low, interaction with olive biomass accumulation that is reduced in response to increased LAI growth rate and then to increased competition for water (−0.23) (Fig. 9a).

TE of both olive trees and grass cover were positively related to the relevant biomass accumulation (0.23 and 0.32), and the increasing TE in response to water stress (RelTE) is positively related to olive tree biomass, thought this effect is low (0.18) (Fig. 9a). Olive biomass is positively related to soil AWC (0.6) and root depth (0.47) (Fig. 9a) while grass growth is almost insensitive to AWC (0.07) and positively correlated to the explored soil depth (0.37) (Fig. 9b), where the negative impact of increasing grass rooting depth on olive tree biomass (−0.18) further emphasizes the effect of the competition for water.

Parameters influencing the response of transpiration and leaf area growth to water stress (a and b parameters in Eq. (22)) indicated that olive biomass accumulation is slightly dependent on these parameters. As expected, increasing values of parameter a reduce olive tree biomass accumulation (−0.13) as the reduction of relative transpiration/leaf area growth to FTSW is positively related to this parameter. The opposite trend is observed for parameter b (0.15), whose increasing values

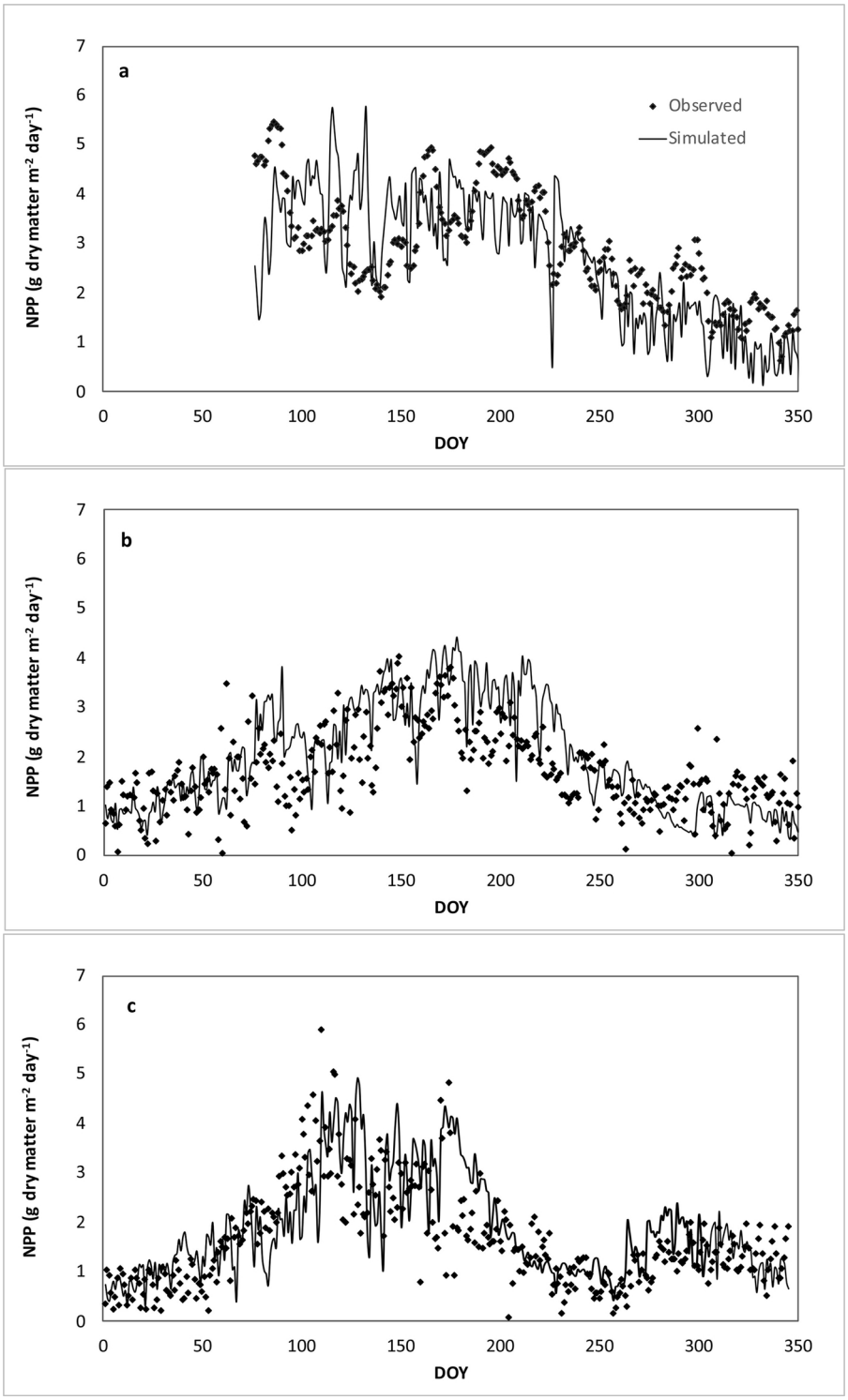

Fig. 3. Daily trend of observed and simulated Net Primary Production (NPP) of S. Paolina olive grove in 2010 (a), 2011 (b) and 2012 (c) at site 1 (described in Table 1 and Fig. 2).

result into a lower impact of FTSW on relative transpiration/leaf area growth (Fig. 9a).

4. Discussion

A new olive grove model, based on process-based algorithms, was designed to simulate phenology, biomass accumulation and yield of olive tree considering water competition with grass cover. This model was conceived bearing in mind two main aspects: (i) it should require a limited input variables and parameters to be potentially applicable in sites with a limited number of observations and at the same time; (ii) it should be robust enough to produce reliable results outside the calibration/validation area.

The simulation approach, originally developed in Sinclair (1986) and Amir and Sinclair (1991) for crops and modified by Bindi et al. (1997, 2005) and Leolini et al. (2018) for grapevine, uses RUE and transpiration efficiency TE as the main parameters driving the simulation of daily dry matter assimilation. The inverse relationship between

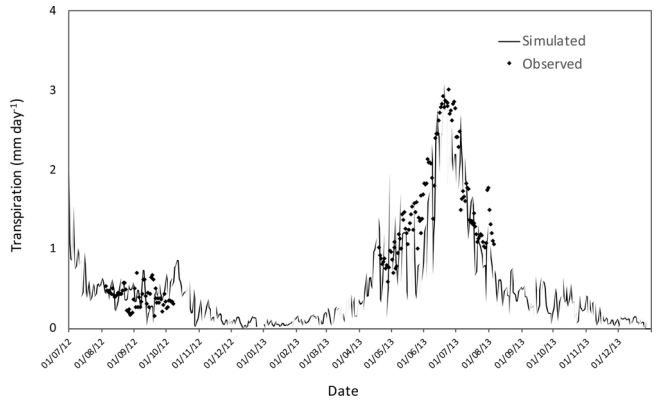

Fig. 4. Daily course of observed and simulated olive tree transpiration (mm day^{-1}) in 2012 and 2013 at site 2 (described in Table 1 and Fig. 2).

TE and VPD (Eq. (16)), that follows the approach proposed by Tanner and Sinclair (1983), is particularly responsive to reproduce the observed effect of VPD on TE but, in its original version proposed by the authors, still lacks of the response of TE to water stress as observed in the field (Villalobos et al., 2012). In the present study, we therefore extended the application of TE under water stress conditions using experimental results of Villalobos et al. (2012) describing how TE increases in responses to increasing water stress.

A simple but straightforward empirical approach was used to describe the relationships between the fraction of transpirable soil water (FTSW) and both leaf area growth (LA) and transpiration (TR) in olive trees for a widely cultivated variety (cv Leccino). The results indicate that, while FTSW thresholds limiting leaf area growth and transpiration are approximately the same (0.32), after this limit leaf area growth starts decreasing at a faster rate with respect to transpiration (Fig. 2 in SI_1). This may further emphasize the productive strategy that olive tree implements under a water stress regime (Tognetti et al., 2009), where expansion of leaves is reduced to avoid water loss and preserve photosynthesis (Casadebaig et al., 2008). This in contrast to the "conservative strategy", which aims at reducing leaf expansion when FTSW is still relatively high (Sinclair and Muchow, 2001).

The few parameters required for the model (Table 2), many of which were found in the literature, simplified the calibration that was limited to three parameters, namely transpiration efficiency coefficient *Kd* for olive tree and grass cover, and LAI growth-rate of grass. This reduction is highly desirable to avoid a model that, having a too large a set of crop-specific parameters to be calibrated, would result in a likely best fit for a particular site but with results that could hardly be extrapolated to another site without readjustment of the model coefficients (Sinclair and Seligman, 2000). In this regard, Tuscany region was

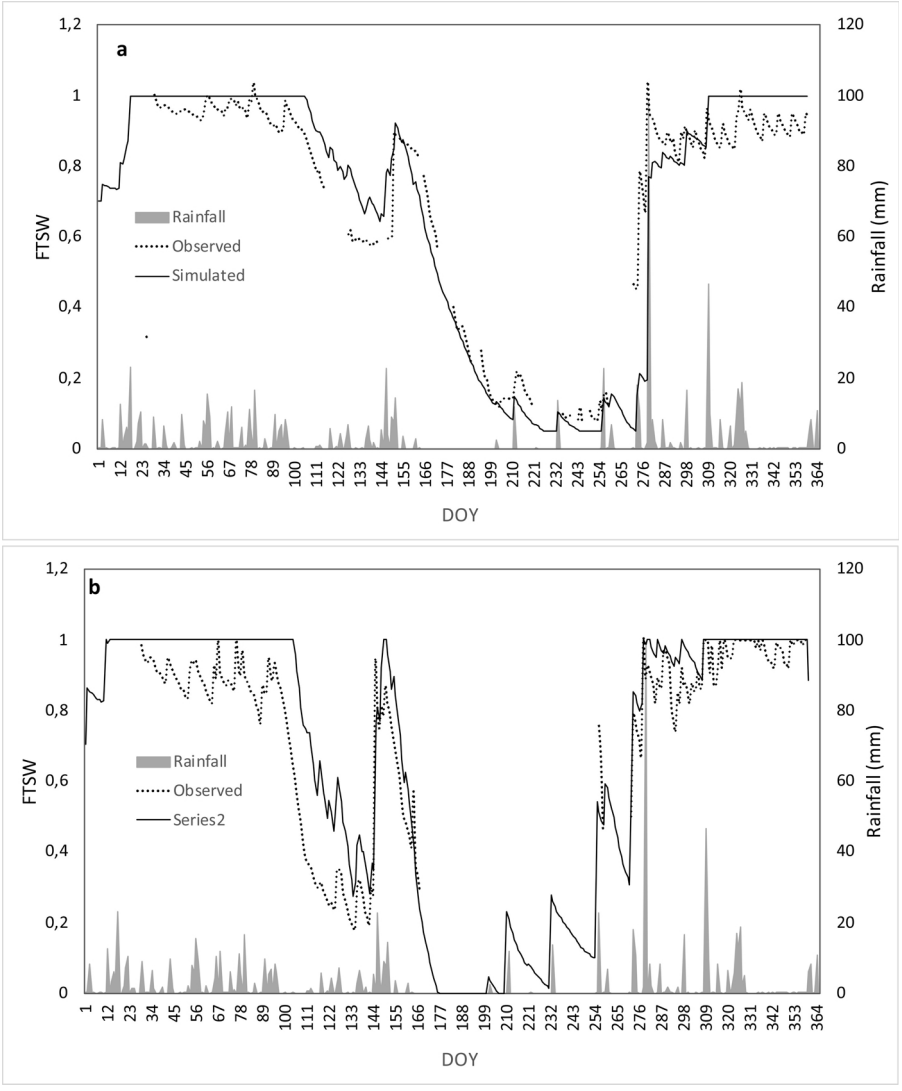

Fig. 5. Daily course of observed and simulated FTSW in 2013 over the entire soil profile (a) and the top layer (b) at site 2 (described in Table 1 and Fig. 2).

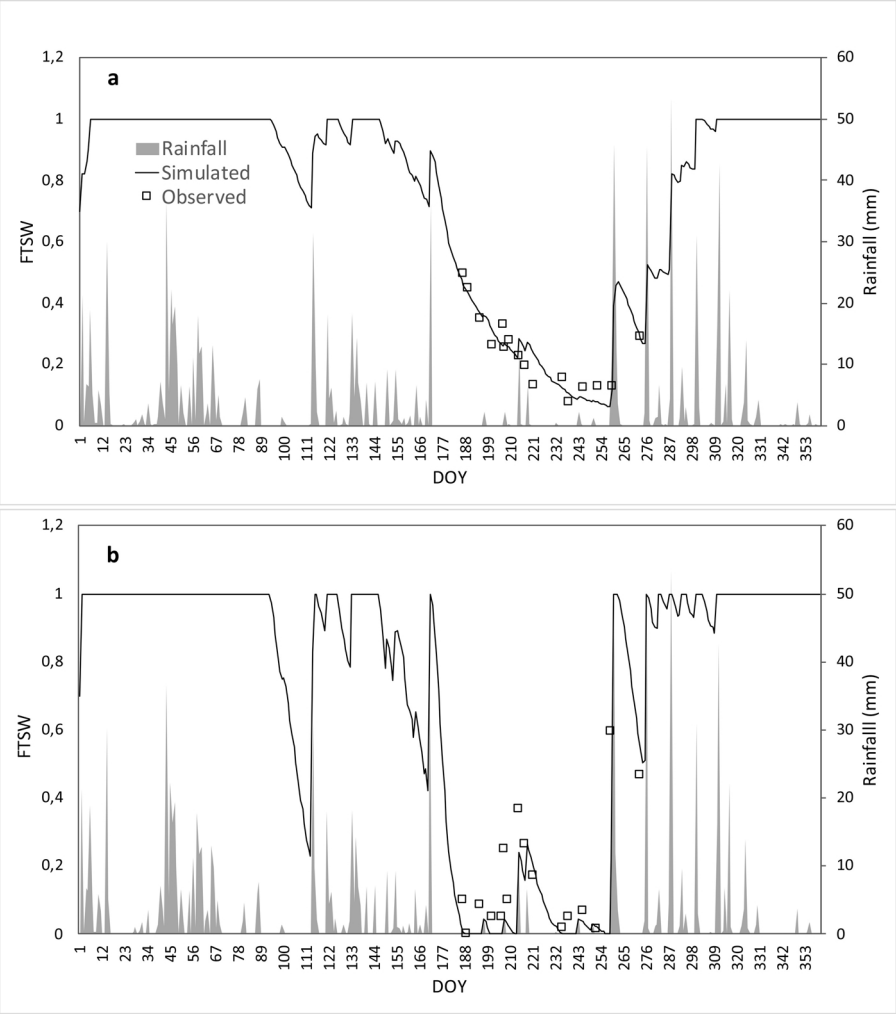

Fig. 6. Daily course of observed and simulated FTSW in 2016 over the entire soil profile (a) and the top layer (b) at site 4 (described in Table 1 and Fig. 2).

selected as testing area for the model since it shows very heterogeneous climatic features as well as soil types and management practices, providing an effective benchmark for model validation outside the calibration area. Its climate ranges from Mediterranean to temperate warm or cool following altitudinal and latitudinal gradients and distance from the sea (Rapetti and Vittorini, 1995, Fig. 2). In particular, the most southern, coastal provinces Grosseto (sites 1, 2, 3, 6) and Livorno (site 8) are the warmest and driest, while the inner provinces Florence (sites 4, 10, 11), Siena (site 13) and Lucca (site 7) have a more continental climate. As a matter of fact, the range of climates used for calibration and validation covers the most common climates typical for olive tree cultivation in Italy (Meso-Mediterranean, Meso-Temperate, Supra-Temperate), which accounts for climates encountered over 80% of its total olive tree cultivated area (Fig. 2).

The results obtained in the calibration and validation tests emphasized the robustness of the model in simulating the assimilation performances of the entire agro-ecosystem, as well as growth and development of the single agro-ecosystem components in conditions differing for plant density, soil texture and management practices. Given the simplified approach and the derived assumptions considered in the model, we retain it as successful result.

Bud-break and flowering dates used for calibrating phenology model were not related to specific varietys but were assumed as representative of the most common varieties grown in Tuscany region (cvs. Frantoio and Moraiolo). This pool of varieties showed in the coastal area a shorter dormancy period that culminated with an earlier bud-break and flowering as compared to inner colder areas. Indeed, bud break occurs 20 days-earlier for warmer site (Follonica, site C in Table 1 of SI_2) as compared to the cooler site (Montepaldi, site B in Table 1 of SI_2). The calibration of our model based on GDH, indicated that this phenomenon is compatible with warmer temperatures occurring in Follonica that promotes an earlier opening of vegetative buds with respect Montepaldi site further confirming the results of López-Bernal et al. (2017) demonstrating that vegetative buds dormant state is easily reversible depending on forcing temperatures.

The flowering stage was simulated accounting for the dormancy period during which the differentiation between vegetative and reproductive buds occurs (De Melo-Abreu et al., 2004; Orlandi et al., 2004; Fabbri and Alerci, 1999). Our results evidenced that the calibrated model was able to detect the differences in the occurrence of anthesis date between sites, where the inner and colder sites (Florence and Prato) are in delay with respect to coastal site (Grosseto), with a good detection of the inter-annual variability for each site. The optimal temperatures for chilling accumulation were lower than 9 °C and this threshold is close to what observed for olive tree in De Melo-Abreu et al. (2004) and Rallo and Martin (1991) that found 7.3 °C and 7.2 °C. The optimal temperatures for forcing accumulation were found higher than 8.5 °C that is in the range of values estimated for olive tree in Galán et al. (2005) (from 6 °C to 12.5 °C) and De Melo-Abreu et al. (2004) (from 8.5 °C to 9.1 °C) in different climates across the Mediterranean basin.

The overall growth model, accounting for ground cover and olive

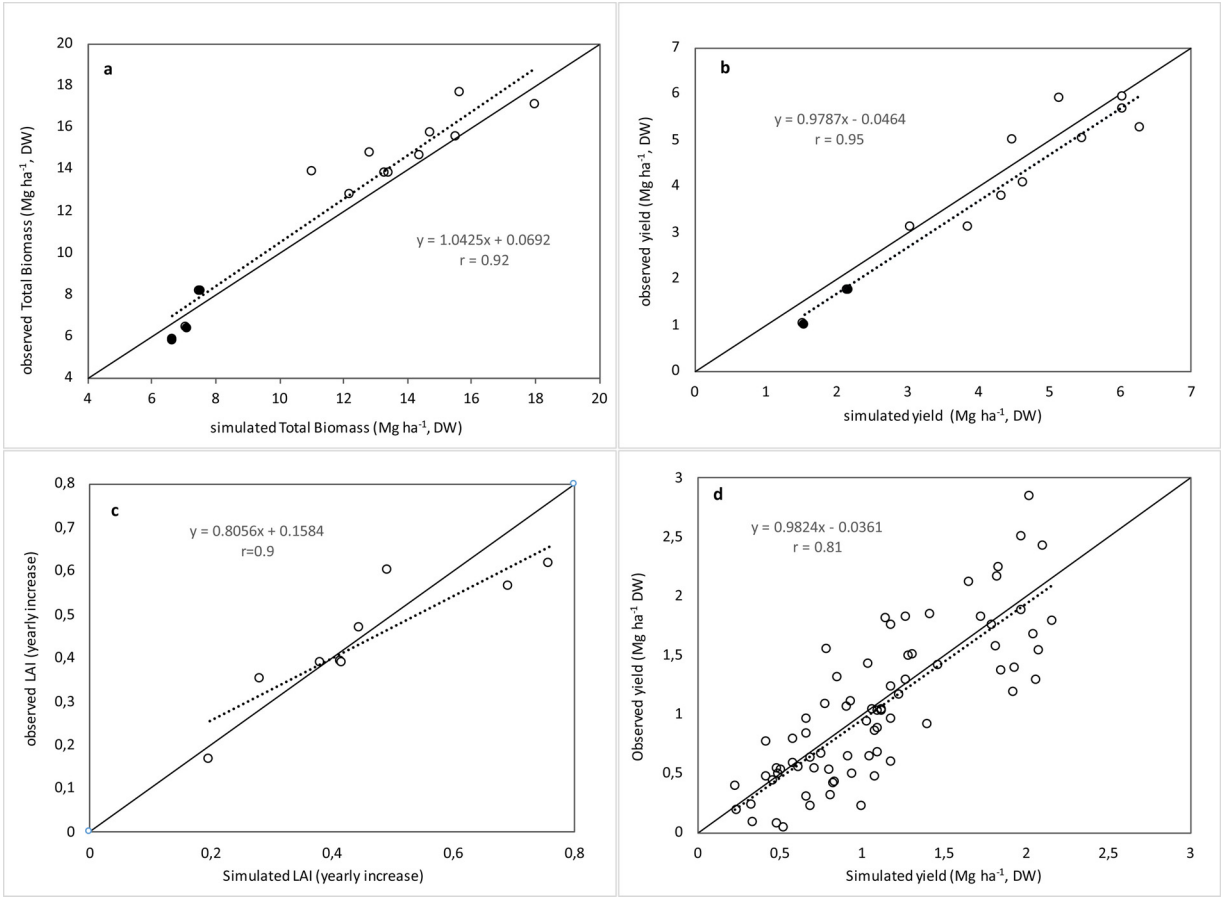

Fig. 7. Correlation between observed and simulated total dry matter (a), final yield (b–d) and yearly LAI increase (c). The dashed line presents the regression line, the continuous line the 1:1 perfect agreement. In subfigure a, closed circles represent yearly cumulated Net Primary Production of the entire ecosystem observed and simulated for sites 1 while open circles represents the yearly total accumulation of olive tree biomass observed and simulated for site 3. In subfigure b, closed circles represents observed and simulated final yield for sites 1 and open circles observed and simulated final yield for site 3. In site 1 data were taken in the period 2010–2012 in rain-fed conditions, in site 3 in the period 2008–2010 under three irrigation treatments. Data are expressed as dry weight (DW) per hectares. In subfigure c, Leaf Area Index (LAI) data are relevant to site 3 for the period 2008–2010 under three irrigation treatments. In subfigure d, yield is expressed as DW and is relevant to sites from 6 to 13. Each site is described in Table 1 and Fig. 2.

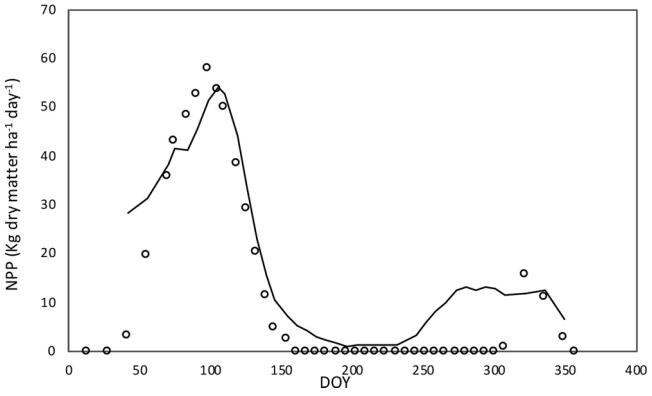

Fig. 8. Daily course of observed and simulated Net Primary Production (NPP) of grass in 1993 at site 5 (described in Table 1 and Fig. 2).

tree layer, was calibrated and validated using carbon flux data from the EC technique. These data are particularly suitable for assessing crop model performances since they take into account the effect of weather and management practices on the ecosystems at the spatial and temporal scale required to evaluate the performances of a process-based model (Brilli et al., 2014, 2017, 2018; Giltrap et al., 2015; Noirot-Cosson et al., 2016; Congreves et al., 2016).

The three years used in the calibration/validation process with EC data in site 1 included 2012 that was close to the long-term average (i.e. 1981–2012) yearly rainfall (626 mm y^{-1}; anomaly = −0.3%), while 2010 and 2011 represent positive (anomaly = +27.4%) and negative extremes (anomaly = −41.3%) (Brilli et al., 2016). As such, we considered a reliable benchmark for testing the model performances under different weather conditions.

The calibration process produced a *Kd* for olive tree (6.5 Pa) that is higher with respect to what observed for grapevine in a Mediterranean climate (*Kd* = 3.8 Pa, Leolini et al., 2018). This supports olive tree efficiency in water use (Xiloyannis et al., 1999) as an effect of physiological adjustments and morphological adaptations (Moreno et al., 1996; Chartzoulakis et al., 1999; d'Andria et al., 2009; Tognetti et al., 2009; Cocozza et al., 2015). *Kd* for grasses was lower than that observed for olive tree (5 Pa) and within the range for C3 species reported in Soltani and Sinclair (2012).

Since from the EC data used in this paper it was not possible to disentangle the dynamics of each single component of the grove, the performances of the calibrated model must be further evaluated in simulating specific processes separately for grass and tree cover (Brilli et al., 2018). Accordingly, the model was tested for grass cover and olive tree biomass accumulation and final yield, olive tree transpiration and water balance considering different climates, plant density and management practices.

The simulation of grass cover growth in site 5, in the absence of competition with olive tree, indicated that the model was able to

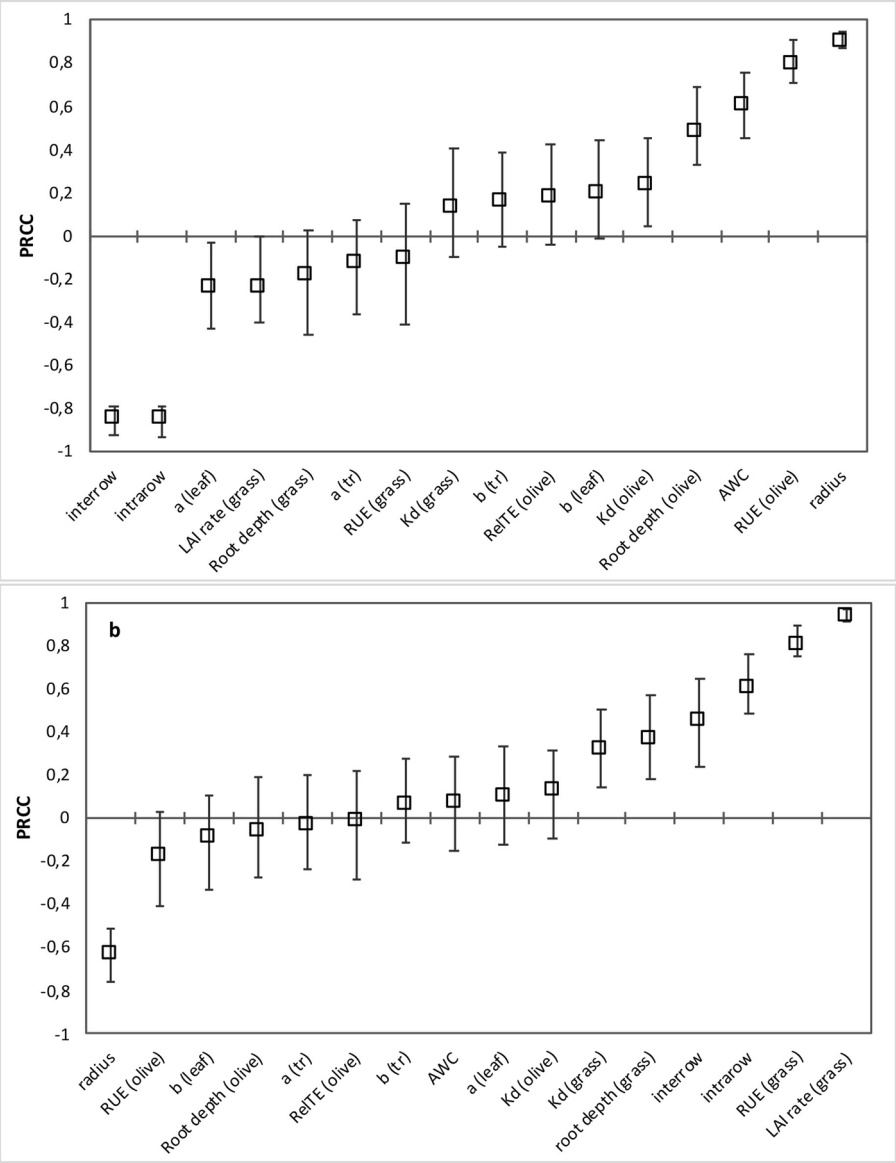

Fig. 9. Model sensitivity analysis. Partial rank correlation coefficient (PRCC) for total cumulated olive tree (a) and grass (b) biomass. Interval of confidence is indicated.

identify the timing and magnitude of maximum growth intensity and the following senescence period. The model simulated grass recovery early in autumn, in advance with respect to observed data, as the effect of prolonged rainy periods in that period. This difference is likely related to the presence in the plot of annual self-reseeding species, such as *Trifolium subterraneum* or *Lolium rigidum*, typical of the Mediterranean area, which after senescence produce seeds that pass the summer buried in the soil (Ghamkhar et al., 2015). This protection mechanism against drought prevents a prompt response of the ground cover to sporadic rainfall events during summer ("false breaks") when optimal conditions for seed growth are not yet reached (Koukoura, 2007). This behavior, as many others that are not properly addressed by many grass models (Calanca et al., 2016), is important for understanding the different responses observed in the field and are of great importance when the simulation should represent competition for water between trees and grasses in dry areas (D'Onofrio et al., 2015).

When the model was applied in site 3, to simulate the competition between grass cover and olive tree under 50% deficit irrigation in 2012, the fraction of NPP partitioned to grass at the end of the season was satisfactorily estimated resulting 25% with respect to 28% as reported in the experiment of Scandellari et al. (2016). Interestingly, when looking at the daily course of observed NPP in 2010, the model was able to reproduce the drop of agroecosystem dry matter production because of soil tillage on DOY 135 that entirely removed the grass layer (simulated by setting LAI of grass to 0 at that date). The assimilation peak observed on DOY 180 was well captured by the model as associated to grass recovery following tillage, joint to assimilation rate of olive tree under favorable soil moisture conditions (Fig. 3a).

Even though our dataset does not allow further comparison and there is still not a consolidated literature on biomass partition between olive trees and grass in groves, some comparisons may be attempted. The results reported in Scandellari et al. (2016) and Nardino et al. (2013) suggest that the contribution of ground cover total cumulated biomass of the system tends to increase as planting density decreases. It passes from 28% for an intensive partially irrigated olive grove of the previous example (513 plants ha^{-1}), to 35% for a fully irrigated low-density grove (250 plants ha^{-1}, Nardino et al. (2013). Our results are in line with this limited set of observations since grass cover biomass partitioning is negatively affected by olive tree plant density (Fig. 9). As an example, when we decreased plant density in site 3 from 513 to

Table 2
List of model variables. Legend: OT = olive tree; GR = grass; SO = soil.

Variable	Description	Layer	Units/value	Reference
State				
DM	Potential cumulated dry matter	OT/GR	$g\,m^{-2}$	
ADM	Actual cumulated dry matter	OT/GR	$g\,m^{-2}$	
LAI	Leaf Area Index	OT/GR	$m^2\,m^{-2}$	
Yield	Yield per hectare	OT/GR	$g\,m^{-2}$	
Rates				
Int.Rad	Intercepted radiation	OT/GR	Rate (0–1)	Testi et al. (2006)
LAI_{inc}	Potential LAI growth	OT	$m^2\,m^{-2}$	
$GLAI_d$	Potential LAI growth	GR	$m^2\,m^{-2}$	Celette et al. (2010)
$ALAI_{inc}$	Actual LAI growth	OT	$m^2\,m^{-2}$	
$AGLAI_d$	Actual LAI growth	GR	$m^2\,m^{-2}$	
SLAId	LAI senescence rate	GR	$m^2\,m^{-2}$	
LAI_rate	Daily growth rate	GR	Rate (0–1)	*Calibrated*
Red_Tr	Effect of FTSW on Transpiration	OT	Rate (0–1)	*Calibrated*
Red_Tr	Effect of FTSW on Transpiration	GR	Rate (0–1)	Schoppach and Sadok (2012)
Red_LAI	Effect of FTSW on LAI growth	OT	Rate (0–1)	*Calibrated*
FTSW	Fraction Transpirable Soil Water	SO	Rate (0–1)	
$FTSW_{reg\_LAI}$	Fraction Transpirable Soil Water (break point)	SO	0.48	Schoppach and Sadok (2012)
ATSW1-2	Actual total soil water	SO	mm	
Tr	Transpiration	OT/GR	$mm\,d^{-1}$	
HI.pot	Harvest index	OT	0.35	Villalobos et al. (2006)
SVEP	Soil evaporation	SO	$mm\,d^{-1}$	
PCf	Partition coefficient to leaves	OT	Rate (0–1)	Mariscal et al. (2000) Morales et al. (2016)
Plant parameters				
vol	Crown volume	OT	m^3	
PlantA	m^2 per plant	OT	m^2	
Root depth	Max explored depth	OT	m	
Root depth	Max explored depth	GR	m	
k'	Olive tree extinction coefficient	OT	Rate (0–1)	Villalobos et al. (2006)
k	Grass cover extinction coefficient	OT	0.5	*Assumed*
RUE	Radiation Use Efficiency	OT	$0.98\,g\,MJ^{-1}\,m^{-2}$	Villalobos et al. (2012)
RUE	Radiation Use Efficiency	GR	$2.2\,g\,MJ^{-1}\,m^{-2}$	Bélanger et al. (1992); Duru et al. (1995)
Kd	Coefficient	OT	6.5 Pa	*Calibrated*
Kd	Coefficient	GR	5 Pa	*Calibrated*
SLA	Specific leaf area	OT	$0.0042\,m^2\,g^{-1}$	Villalobos et al. (2006)
LAD	Leaf Area Density	OT	$m^2\,m^{-3}$	
Soil parameters				
TTSW	Total Transpirable Soil Water	SO	mm	
AWC	Available Water Content	SO	mm	
Environmental parameters				
Tmin	Minimum daily temperature		°C	
Tmax	Maximum daily temperature		°C	
Rainfall	Daily cumulated rainfall		mm	
Radiation	Daily global radiation		MJ	
VPD	Vapor Pressure Deficit		kPa	

256 plants ha^{-1} in a fully irrigated treatment to reproduce the experiment in Nardino et al. (2013), NPP partitioning to ground cover increased from 23% to 37%, which is fully comparable to what was observed in that experiment where grass cover represented 35% of total NPP.

The robustness of the model was further emphasized by its capacity to simulate specific processes such as olive tree transpiration and water dynamics, biomass accumulation and leaf area growth. In sites 2 and 4, the model faithfully simulated the olive tree transpiration and FTSW, demonstrating the ability of the model to reproduce the actual evapotranspiration for different plant density, climate and soil. RMSE obtained for olive tree transpiration (0.43 mm) is in line with the results of López-Bernal et al. (2018) (0.32 mm) and Villalobos et al. (2013) (0.32 mm). The model also well reproduced the effect of grasses and olive trees competition for water in the top layer and more in general through the entire soil profile.

Overall, the model accurately reproduced total biomass accumulation and final yield of an intensive grove with three irrigation treatments (site 3, Table 2) with a relevant RMSE of 1.2 and 0.58 Mg ha^{-1}, where also the annual increase of LAI was well simulated with an RMSE of 0.07.

These good performances on experimental plots were corroborated when the model was applied for yield estimation on farm level on sites 6–13. In particular, yield data for these sites exhibited a general trend for alternate bearing that was captured by the model with a good level of agreement with observations, especially considering that physiology of alternate bearing is not still fully understood (Dag et al., 2010). Interestingly, in some case, we observed an interaction between the alternate bearing and the effect of stress events at anthesis that may further depress the expected reduced yield or smooth the expected increased yield (e.g. Fig. 7 in SI_2). This supports the importance of the simulation of these stressing events for a correct yield estimation (Lorite et al., 2018).

Despite the good performances of the model in different environmental conditions, some drawbacks and warnings in the use of present model due to a specific parametrization must be highlighted.

There is still a lack in the understanding of processes underlying the release of bud break (López-Bernal et al., 2017) and this limits the application of the proposed model. Further, the model we proposed only accounts for the difference in the occurrence of bud break between

Table 3
Goodness of fit indicators for simulations over sites 1–13.

Site	Variable	Period	Aggregation	*r*	RMSE	RRMSE	MBE	MAE
1	NPP (grass + olive tree)	2010	ten days (C)	0.81	7.6 g m^{-2}	17%	−1.45 g m^{-2}	6.4 g m^{-2}
1	NPP (grass + olive tree)	2011	ten days (C)	0.85	6.8 g m^{-2}	23%	−0.9 g m^{-2}	5.4 g m^{-2}
1	NPP (grass + olive tree)	2012	ten days (C)	0.82	5.6 g m^{-2}	16%	−1.8 g m^{-2}	4.4 g m^{-2}
2	FTSW	2013	ten days (A)	0.95	11.0%	11%	−4.7%	8.3%
2	FTSW1	2013	ten days (A)	0.94	7.7%	7.7%	3.6%	6.5%
2	Transpiration (olive tree)	2012–2013	day	0.86	0.43 mm	15%	−0.16 mm	0.33 mm
1–3	Yield	2008–2010, 2012 (site 3) 2010, 2012 (site 1)	year	0.95	0.58 Mg ha^{-1}	11%	0.30 Mg ha^{-1}	0.52 Mg ha^{-1}
1–3	Total biomass	2008–2010, 2012 (site3) 2010–2012 (site 1)	year	0.92	1.2 Mg ha^{-1}	10%	−0.47 Mg ha^{-1}	0.90 Mg ha^{-1}
3	LAI (olive tree)	2008–2010	year	0.9	0.07	17%	0.013	0.06
4	FTSW	2016	day	0.94	6.5%	6.5%	2.3%	5.1%
4	FTSW1	2016	day	0.91	10%	10%	−7.5%	7.3%
5	NPP (grass)	1993	week (A)	0.96	5.6 kg ha^{-1} day^{-1}	11%	2.7 kg ha^{-1} day^{-1}	4.45 kg ha^{-1} day^{-1}
6–13	Yield	1970–2006$^{\mu}$	year	0.81	0.41 Mg ha^{-1}	18%	0.05 Mg ha^{-1}	0.3 Mg ha^{-1}

FTSW1 relates to data from the 0 to 30 cm layer, FTSW relates to the entire soil layer. Under the field *period*, μ indicates the first year and the last year considering all the sites. In the *aggregation* field, C = cumulated, A = averaged. *r* is significant for $P < 0.01$ in any case. NPP and biomass are expressed as dry matter.

sites with contrasting climates, but still lack a validation in estimating the inter-annual variability of this stage since the relevant data were provided as average DOY for both Florence and Follonica. More in general, given the large influence of climatic conditions on the parametrization of the phenology model, further calibrations for its application outside the range of conditions where it was developed are required.

The model does not consider the carry-over effect of water stress, which may lead to a reduction in the number of flowers and fruit set in the year following the drought event (Caruso et al., 2013). However this effect is erratic (e.g. Sillari et al., 1993; Gucci et al., 2007; Caruso et al., 2013) and the poor understanding of underlying physiological processes makes the modelling difficult. Further, the model assumes a spatial uniform distribution of olive tree and grass roots density in the first soil layer, while the distribution of roots of olive tree varies depending on the distance from the trunk (Rallo and Provenzano, 2013). This may results into a poor simulation of the competition for water especially as increases the sampling distance from the trunk.

The use of empirical approach describing the effect of FTSW on olive transpiration requires, in any case, a different parametrization depending on the varieties that may exhibit different tolerance to water stress (Cola et al., 2014; Alfieri et al., 2018). As an example, transpiration of cv “Coratina” grown in pots (Sofo et al., 2008) showed a higher susceptibility to water stress than cv Leccino (this study), while cv “Nocellara del Belice (Rallo and Provenzano, 2013) showed an intermediate response (Fig. 8 in SI_2).

The sub-model describing the effect of heat and water stress at anthesis of final yield must be refined as in the present model it is based on a limited number of observation to date present in literature. In particular, the maximum temperature leading to a null fruit set in Eq. (36) is based on a laboratory experiment on pollen germination (Koubouris et al., 2009), while field experiments on this issue are still lacking.

The sensitivity analysis highlighted that olive tree growth is highly responsive to light interception parameters (planting density, crown radius) and actually the model provided the highest simulation performances when this information was available at a high spatial and temporal resolution (as in site 3, Fig. 7a and b). When the model was feed with a lower quality data of ground cover as obtained from not updated low-resolution imageries, the performances were significantly reduced (sites 6–13 Fig. 7d, Table 3). This implies that these parameters cannot be easily assumed but should actually reflect the current situation in the olive grove. Proximal sensing data from an unmanned aerial vehicle (UAV) could be exploited for such a purpose to derive the geometrical parameters of the canopy and LAI at the highest spatial resolution (Caruso et al., 2017, 2019; Zarco-Tejada et al., 2014; Matese et al., 2017).

5. Conclusion

The objective of this work was to develop and validate a growth model simulating growth of olive trees and grass cover. The model was calibrated and validated in Tuscany region over sites encompassing different types of Mediterranean climate, soil and management practices. The effect of heat and water stress at anthesis were also considered as yield reducing factors and the impact of alternate bearing was also simulated.

Overall, despite having a simple architecture, it faithfully simulated different processes, including olive tree phenology, plant transpiration and total biomass accumulation and partitioning at both tree and grass level. Further, the model was able to reproduce final yield at farm level and can be therefore considered as a tool for monitoring the current status of growing season as well as to test the effectiveness of management practices for improving economic viability of olive tree cultivation, even with a limited set of input parameters.

Acknowledgment

This research was supported by the LIFE project ADAPT2CLIMA ref: LIFE14 CCA/GR/000928. The authors wish to thank the anonymous referees for their helpful comments on the first draft of the manuscript.

Appendix A. Supplementary data

Supplementary data associated with this article can be found, in the online version, at https://doi.org/10.1016/j.eja.2019.02.002.

References

Alfieri, S.M., Riccardi, M., Menenti, M., Basile, A., Bonfante, A., De Lorenzi, F., 2018. Adaptability of global olive cultivars to water availability under future Mediterranean climate. Mitig. Adapt. Strat. Glob. Change 1–32.
Amir, J., Sinclair, T.R., 1991. A model of water limitation on spring wheat growth and yield. Field Crop Res. 28 (1–2), 59–69.
Argenti, G., Cervasio, F., Ponzetta, M., 2012. Control of bracken (*Pteridium aquilinum*) and feeding preferences in pastures grazed by wild ungulates in an area of the Northern Apennines (Italy). Ital. J. Anim. Sci. 11 (4), 336–341.
Bélanger, G., Gastal, F., Lemaire, G., 1992. Growth of a tall fescue sward fertilized with different rates of nitrogen. Crop Sci. 32 (6), 1371–1376.
Benlloch-González, M., Sánchez-Lucas, R., Benlloch, M., Ricardo, F.E., 2018. An approach to global warming effects on flowering and fruit set of olive trees growing under field conditions. Sci. Hortic. 240, 405–410.
Bindi, M., Bellesi, S., Orlandini, S., Fibbi, L., Moriondo, M., Sinclair, T., 2005. Influence of water deficit stress on leaf area development and transpiration of *Sangiovese grapevines* grown in pots. Am. J. Enol. Viticult. 56 (1), 68–72.
Bindi, M., Miglietta, F., Gozzini, B., Orlandini, S., Seghi, L., 1997. A simple model for simulation of growth and development in grapevine (*Vitis vinifera* L.). II. Model validation. Vitis 36, 73–76.
Brilli, L., Gioli, B., Toscano, P., Moriondo, M., Zaldei, A., Cantini, C., Ferrise, R., Bindi, M., 2016. Rainfall regimes control C-exchange of Mediterranean Olive orchard. Agric.

Ecosyst. Environ. 233, 147–157.
Brilli, L., et al., 2017. Review and analysis of strengths and weaknesses of agro-ecosystem models in representing C and N fluxes. Sci. Total Environ. 598, 445–470.
Brilli, L., Chiesi, M., Maselli, F., Moriondo, M., Gioli, B., Toscano, P., Zaldei, A., Bindi, M., 2013. Simulation of olive grove gross primary production by the combination of ground and multi-sensor satellite data. Int. J. Appl. Earth Obs. Geoinf. 23, 29–36.
Brilli, L., Ferrise, R., Lugato, E., Moriondo, M., Bindi, M., 2014. Using mitigation and adaptation strategies to optimize crop yield and greenhouse gas emissions. In: Maren Oelbermann (Ed.), Sustainable Agroecosystems in Climate Change Mitigation. Wageningen Academic Publisher, Netherland ISBN: 978-90-8686-235-1.
Brilli, L., Lugato, E., Moriondo, M., Gioli, B., Toscano, P., Zaldei, A., Leolini, L., Cantini, C., Caruso, G., Gucci, R., Merante, P., Dibari, C., Ferrise, R., Bindi, M., Costafreda-Aumedes, S., 2018. Carbon sequestration capacity and productivity responses of Mediterranean olive groves under future climates and management options. Mitig. Adapt. Strat. Glob. Change 1–25.
Calanca, P., Deléglise, C., Martin, R., Carrère, P., Mosimann, E., 2016. Testing the ability of a simple grassland model to simulate the seasonal effects of drought on herbage growth. Field Crop Res. 187, 12–23.
Cantini, C., Cimato, A., Sani, G., 1999. Morphological evaluation of olive germplasm present in Tuscany region. Euphytica 109, 173–181.
Caruso, G., Rapoport, H.F., Gucci, R., 2013. Long-term evaluation of yield components of young olive trees during the onset of fruit production under different irrigation regimes. Irrig. Sci. 31 (1), 37–47.
Caruso, G., Tozzini, L., Rallo, G., Primicerio, J., Moriondo, M., Palai, G., Gucci, R., 2017. Estimating biophysical and geometrical parameters of grapevine canopies ('Sangiovese') by an unmanned aerial vehicle (UAV) and VIS-NIR cameras. Vitis 56 (2), 63–70.
Caruso, G., Zarco-Tejada, P.J., González-Dugo, V., Moriondo, M., Tozzini, L., Palai, G., Rallo, G., Hornero, A., Primicerio, J., Gucci, R., 2019. High-resolution imagery acquired from an unmanned platform to estimate biophysical and geometrical parameters of olive trees under different irrigation regimes. PLoS One 14 (1), e0210804.
Casadebaig, P., Debaeke, P., Lecoeur, J., 2008. Thresholds for leaf expansion and transpiration response to soil water deficit in a range of sunflower genotypes. Eur. J. Agron. 28, 646–654.
Celette, F., Ripoche, A., Gary, C., 2010. WaLIS—a simple model to simulate water partitioning in a crop association: the example of an intercropped vineyard. Agric. Water Manage. 97 (11), 1749–1759.
Challinor, A.J., Wheeler, T.R., Craufurd, P.Q., Slingo, J.M., Grimes, D.I.F., 2004. Design and optimization of a large-area process-based model for annual crops. Agric. For. Meteorol. 124 (1), 99–120.
Chartzoulakis, K., Patakas, A., Bosabalidis, A.M., 1999. Changes in water relations, photosynthesis and leaf anatomy induced by intermittent drought in two olive cultivars. Environ. Exp. Bot. 42 (2), 113–120.
Chuine, I., 2000. A unified model for budburst of trees. J. Theor. Biol. 207 (3), 337–347.
Chuine, I., Cour, P., Rousseau, D.D., 1999. Selecting models to predict the timing of flowering of temperate trees: implications for tree phenology modelling. Plant Cell Environ. 22 (1), 1–13.
Cocozza, C., Marino, G., Giovannelli, A., Cantini, C., Centritto, M., Tognetti, R., 2015. Simultaneous measurements of stem radius variation and sap flux density reveal synchronization of water storage and transpiration dynamics in olive trees. Ecohydrology 8 (1), 33–45.
Cola, G., Mariani, L., Salinari, F., Civardi, S., Bernizzoni, F., Gatti, M., Poni, S., 2014. Description and testing of a weather-based model for predicting phenology, canopy development and source–sink balance in *Vitis vinifera* L. cv. Barbera. Agric. For. Meteorol. 184, 117–136.
Confalonieri, R., Bellocchi, G., Bregaglio, S., Donatelli, M., Acutis, M., 2010. Comparison of sensitivity analysis techniques: a case study with the rice model WARM. Ecol. Model. 221 (16), 1897–1906.
Congreves, K.A., Grant, B.B., Dutta, B., Smith, W.N., Chantigny, M.H., Rochette, P., Desjardins, R.L., 2016. Predicting ammonia volatilization after field application of swine slurry: DNDC model development. Agric. Ecosyst. Environ. 219, 179–189.
d'Andria, R., Lavini, A., Morelli, G., Sebastiani, L., Tognetti, R., 2009. Physiological and productive responses of *Olea europaea* L. cultivars Frantoio and Leccino to a regulated deficit irrigation regime. Plant Biosyst. 143, 222–231.
Dag, A., Bustan, A., Avni, A., Tzipori, I., Lavee, S., Riov, J., 2010. Timing of fruit removal affects concurrent vegetative growth and subsequent return bloom and yield in olive (*Olea europaea* L.). Sci. Hortic. 123, 469–472. https://doi.org/10.1016/j.scienta.2009.11.014.
De Melo-Abreu, J.P., Barranco, D., Cordeiro, A.M., Tous, J., Rogado, B.M., Villalobos, F.J., 2004. Modelling olive flowering date using chilling for dormancy release and thermal time. Agric. For. Meteorol. 125 (1), 117–127.
D'Onofrio, D., Baudena, M., D'Andrea, F., Rietkerk, M., Provenzale, A., 2015. Tree-grass competition for soil water in arid and semiarid savannas: the role of rainfall intermittency. Water Resour. Res. 51 (1), 169–181.
Duarte, F., Jones, N., Fleskens, L., 2008. Traditional olive orchards on sloping land: sustainability or abandonment? J. Environ. Manage. 89 (2), 86–98.
Duru, M., Ducrocq, H., Tirilly, V., 1995. Modeling growth of cocksfoot *(Dactylis glomerata* L.) and tall fescue (*Festuca arundinacea* shreb.) at the end of spring in relation to herbage nitrogen status. J. Plant Nutr. 18 (10), 2033–2047.
Fabbri, A., Alerci, L., 1999. Reproductive and vegetative bud differentiation in *Olea europaea* L. J. Hortic. Sci. Biotechnol. 74, 522–527.
Fernández, J.E., Diaz-Espejo, A., d'Andria, R., Sebastiani, L., Tognetti, R., 2008. Potential and limitations of improving olive orchard design and management through modelling. Plant Biosyst. 142, 130–137.
Ferrise, R., Moriondo, M., Trombi, G., Miglietta, F., Bindi, M., 2013. Climate change impacts on typical Mediterranean crops and evaluation of adaptation strategies to cope with. Regional Assessment of Climate Change in the Mediterranean. Springer, Netherlands, pp. 49–70.
Fleskens, L., Duarte, F., Eicher, I., 2008. A conceptual framework for the assessment of multiple functions of agro-ecosystems: a case study of Trás-os-Montes olive groves. J. Rural Stud. 25 (1), 141–155.
Galán, C., García-Mozo, H., Vázquez, L., Ruiz, L., De La Guardia, C.D., Trigo, M.M., 2005. Heat requirement for the onset of the *Olea europaea* L. pollen season in several sites in Andalusia and the effect of the expected future climate change. Int. J. Biometeorol. 49 (3), 184–188.
Gardin, L., Vinci, A., 2006. Carta dei suoli della Regione Toscana in scala-1:250.000. http://sit.lamma.rete.toscana.it/websuoli/.
Ghamkhar, K., Nichols, P.G.H., Erskine, W., Snowball, R., Murillo, M., Appels, R., Ryan, M.H., 2015. Hotspots and gaps in the world collection of subterranean clover (*Trifolium subterraneum* L.). J. Agric. Sci. 153 (6), 1069–1083.
Giltrap, D.L., Vogeler, I., Cichota, R., Luo, J., van der Weerden, T.J., de Klein, C.A.M., 2015. Comparison between APSIM and NZ-DNDC models when describing N-dynamics under urine patches. N. Z. J. Agric. Res. 58 (2), 131–155.
Gucci, R., Lodolini, E.M., Rapoport, H.F., 2007. Productivity of olive trees with different water status and crop load. J. Hortic. Sci. Biotechnol. 82 (4), 648–656.
Iraldo, F., Testa, F., Bartolozzi, I., 2013. An application of Life Cycle Assessment (LCA) as a green marketing tool for agricultural products: the case of extra-virgin olive oil in Val di Cornia, Italy. J. Environ. Plan. Manage. 57 (1), 78–103.
Koubouris, G.C., Metzidakis, I.T., Vasilakakis, M.D., 2009. Impact of temperature on olive (*Olea europaea* L.) pollen performance in relation to relative humidity and genotype. Environ. Exp. Bot. 67, 209–214.
Koukoura, Z., 2007. Natural grasslands – a case study in Greece. In: In: Marschner, P., Rengel, Z. (Eds.), Nutrient Cycling in Terrestrial Ecosystems. Soil Biology Vol. 10 Springer, Berlin, Heidelberg.
Lavee, S., 2007. Biennial bearing in olive (*Olea europaea*). Annales Ser. His. Nat. 17, 101–112.
Leolini, L., Bregaglio, S., Moriondo, M., Ramos, M.C., Bindi, M., Ginaldi, F., 2018. A model library to simulate grapevine growth and development: software implementation, sensitivity analysis and field level application. Eur. J. Agron. 99, 92–105.
López-Bernal, A., Villalobos, F.J., García-Tejera, O., Testi, L., Orgaz, F., 2017. Do olive vegetative buds undergo a real dormant state in winter? Acta Hortic. 1160, 227–230.
López-Bernal, Á., Morales, A., García-Tejera, O., Testi, L., Orgaz, F., De Melo-Abreu, J.P., Villalobos, F.J., 2018. OliveCan: a process-based model of development, growth and yield of olive orchards. Front. Plant Sci. 9, 632.
Lorite, I.J., Gabaldón-Leal, C., Ruiz-Ramos, M., Belaj, A., de la Rosa, R., León, L., Santos, C., 2018. Evaluation of olive response and adaptation strategies to climate change under semi-arid conditions. Agric. Water Manage. 204, 247–261.
Loumou, A., Giourga, C., 2003. Olive groves: the life and identity of the Mediterranean. Agric. Human Values 20 (1), 87–95.
Mancuso, S., Pasquali, G., Fiorino, P., 2002. Phenology modelling and forecasting in olive (*Olea europaea* L.) using artificial neural networks. Adv. Hortic. Sci. 16, 155–164.
Mariscal, M.J., Orgaz, F., Villalobos, F.J., 2000. Radiation-use efficiency and dry matter partitioning of a young olive (*Olea europaea*) orchard. Tree Physiol. 20 (1), 65–72.
Maselli, F., Chiesi, M., Brilli, L., Moriondo, M., 2012. Simulation of olive fruit yield in Tuscany through the integration of remote sensing and ground data. Ecol. Model. 244, 1–12.
Matese, A., Di Gennaro, S.F., Berton, A., 2017. Assessment of a canopy height model (CHM) in a vineyard using UAV-based multispectral imaging. Int. J. Remote Sens. 38 (8–10), 2150–2160.
Metropolis, N., Rosenbluth, A.W., Rosenbluth, M.N., Teller, A.H., Teller, E., 1953. Equation of state calculations by fast computing machines. J. Chem. Phys. 21 (6), 1087–1092.
Monteith, J.L., 1996. The quest for balance in crop modeling. Agron. J. 88 (5), 695–697.
Morales, A., Leffelaar, P.A., Testi, L., Orgaz, F., Villalobos, F.J., 2016. A dynamic model of potential growth of olive (*Olea europaea* L.) orchards. Eur. J. Agron. 74, 93–102.
Moreno, F., Fernandez, E., Clothier, B.E., Green, S.R., 1996. Transpiration and root water uptake by olive trees. Plant Soil 184 (1), 85–96.
Moriana, A., Orgaz, F., Pastor, M., Fereres, E., 2003. Yield responses of a mature olive orchard to water deficits. J. Am. Soc. Hortic. Sci. 128 (3), 425–431.
Moriondo, M., Ferrise, R., Trombi, G., Brilli, L., Dibari, C., Bindi, M., 2015. Modelling olive trees and grapevines in a changing climate. Environ. Model. Softw. 72, 387–401.
Moriondo, M., Orlandini, S., De Nuntiis, P., Mandrioli, P., 2001. Effect of agrometeorological parameters on the phenology of pollen emission and production of olive trees (*Olea europea* L.). Aerobiologia 17 (3), 225–232.
Moriondo, M., Stefanini, F.M., Bindi, M., 2008. Reproduction of olive tree habitat suitability for global change impact assessment. Ecol. Model. 218 (1), 95–109.
Moriondo, M., Trombi, G., Ferrise, R., Brandani, G., Dibari, C., Ammann, C.M., Mariotti Lippi, M., Bindi, M., 2013. Olive trees as bio-indicators of climate evolution in the Mediterranean Basin. Glob. Ecol. Biogeogr. 22 (7), 818–833.
Nardino, M., Pernice, F., Rossi, F., Georgiadis, T., Facini, O., Motisi, A., Drago, A., 2013. Annual and monthly carbon balance in an intensively managed Mediterranean olive orchard. Photosynthetica 51 (1), 63–74.
Nieto, O.M., Castro, J., Fernández, E., Smith, P., 2010. Simulation of soil organic carbon stocks in a Mediterranean olive grove under different soil-management systems using the RothC model. Soil Use Manage. 26 (2), 118–125.
Noirot-Cosson, P.E., Vaudour, E., Gilliot, J.M., Gabrielle, B., Houot, S., 2016. Modelling the long-term effect of urban waste compost applications on carbon and nitrogen dynamics in temperate cropland. Soil Biol. Biochem. 94, 138–153.
Orlandi, F., Garcia-Mozo, H., Dhiab, A.B., Galán, C., Msallem, M., Romano, B., Abichou, M., Dominguez-Vilches, E., Fornaciari, M., 2013. Climatic indices in the

interpretation of the phenological phases of the olive in Mediterranean areas during its biological cycle. Clim. Change 116 (2), 263–284.
Orlandi, F., Garcia-Mozo, H., Ezquerra, L.V., Romano, B., Dominguez, E., Galan, C., Fornaciari, M., 2004. Phenological olive chilling requirements in Umbria (Italy) and Andalusia (Spain). Plant Biosyst. 138 (2), 111–116.
Palese, A.M., Pergola, M., Favia, M., Xiloyannis, C., Celano, G., 2013. A sustainable model for the management of olive orchards located in semi-arid marginal areas: some remarks and indications for policy makers. Environ. Sci. Policy 27, 81–90.
Pearce, S.C., Dobersek-Urbanc, S., 1967. The measurement of irregularity in growth and cropping. J. Hortic. Sci. 42, 295–305. https://doi.org/10.1080/00221589.1967.11514216.
Ponti, L., Gutierrez, A.P., Ruti, P.M., Dell'Aquila, A., 2014. Fine-scale ecological and economic assessment of climate change on olive in the Mediterranean Basin reveals winners and losers. PNAS 111 (15), 5598–5603.
Reichstein, M., et al., 2005. On the separation of net ecosystem exchange into assimilation and ecosystem respiration: review and improved algorithm. Global Change Biol. 11 (9), 1–16.
Rallo, G., Provenzano, G., 2013. Modelling eco-physiological response of table olive trees (*Olea europaea* L.) to soil water deficit conditions. Agric. Water Manage. 120, 79–88.
Rallo, L., Martin, G.C., 1991. The role of chilling in releasing olive floral buds from dormancy. J. Am. Soc. Hortic. Sci. 116, 1058–1062.
Rapetti, F., Vittorini, S., 1995. Carta climatica della Toscana. Pacini Editore, Pisa, Italy.
Rapoport, H.F., Hammami, S.B., Martins, P., Pérez-Priego, O., Orgaz, F., 2012. Influence of water deficits at different times during olive tree inflorescence and flower development. Environ. Exp. Bot. 77, 227–233.
Rapoport, H.F., 2014. The reproductive biology of the olive tree and its relationship to extreme environmental conditions. VII International Symposium on Olive Growing 1057 41–50.
Rivas-Martınez, S., Penas, A., Diaz, T.E., 2004. Bioclimatic Map of Europe – Bioclimates. Cartographic Service, University of Leon. Available from https://webs.ucm.es/info/cif/form/tb_med.htm (retrieved 16.12.13).
Sarvas, R., 1974. Investigations on the annual cycle of development of forest trees. II. Autumn dormancy and winter dormancy. Commun. Inst. For Fenn. 84, 1–101.
Saxton, K.E., Rawls, W., Romberger, J.S., Papendick, R.I., 1986. Estimating generalized soil–water characteristics from texture 1. Soil Sci. Soc. Am. J. 50 (4), 1031–1036.
Scandellari, F., Caruso, G., Liguori, G., Meggio, F., Palese, A.M., Zanotelli, D., Celano, G., Gucci, R., Inglese, P., Pitacco, A., Tagliavini, M., 2016. A survey of carbon sequestration potential of orchards and vineyards in Italy. Eur. J. Hortic. Sci. 81 (2), 106–114.
Schoppach, R., Sadok, W., 2012. Differential sensitivities of transpiration to evaporative demand and soil water deficit among wheat elite cultivars indicate different strategies for drought tolerance. Environ. Exp. Bot. 84, 1–10.
Sillari, B., Cantini, C., Cimato, A., Fiorino, P., 1993. Olive production in the coastal environment of metalliferous hill country. Olivae 47, 39–45.
Sinclair, T.R., 1986. Water and nitrogen limitations in soybean grain production. I. Model development. Field Crops Res. 15 (2), 125–141.
Sinclair, T.R., Hammond, L.C., Harrison, J., 1998. Extractable soil water and transpiration of soybean on sandy soils. Agron. J. 90 (3), 363–368.
Sinclair, T.R., Muchow, R.C., 2001. System analysis of plant traits to increase grain yield on limited water supplies. Agron. J. 93, 263–270.
Sinclair, T.R., Seligman, N.A., 2000. Criteria for publishing papers on crop modeling. Field Crop Res. 68 (3), 165–172.
Sinclair, T.R., Tanner, C.B., Bennett, J.M., 1984. Water-use efficiency in crop production. Bioscience 34 (1), 36–40.
Sofo, A., Manfreda, S., Fiorentino, M., Dichio, B., Xiloyannis, C., 2008. The olive tree: a paradigm for drought tolerance in Mediterranean climates. Hydrol. Earth Syst. Sci. Discuss. 12 (1), 293–301.
Soltani, A., Sinclair, T.R., 2011. A simple model for chickpea development, growth and yield. Field Crop Res. 124 (2), 252–260.
Soltani, A., Sinclair, T.R., 2012. Modeling physiology of crop development, growth and yield. CABI.
Tanner, C.B., Sinclair, T.R., et al., 1983. Efficient water use in crop production: research or research. In: Taylor, H. (Ed.), Limitations to Efficient Water Use in Crop Production. American Society Agronomy, Madison, pp. 1–28.
Testi, L., Villalobos, F.J., Orgaz, F., Fereres, E., 2006. Water requirements of olive orchards: I simulation of daily evapotranspiration for scenario analysis. Irrig. Sci. 24 (2), 69–76.
Tognetti, R., Giovannelli, A., Lavini, A., Morelli, G., Fragnito, F., d'Andria, R., 2009. Assessing environmental controls over conductance through the soil-plant-atmosphere continuum in an experimental olive tree plantation of southern Italy. Agric. For. Meteorol. 149 (8), 1229–1243.
Villalobos, F.J., Perez-Priego, O., Testi, L., Morales, A., Orgaz, F., 2012. Effects of water supply on carbon and water exchange of olive trees. Eur. J. Agron. 40, 1–7.
Villalobos, F.J., Testi, L., Hidalgo, J., Pastor, M., Orgaz, F., 2006. Modelling potential growth and yield of olive (*Olea europaea* L.) canopies. Eur. J. Agron. 24 (4), 296–303.
Villalobos, F.J., Testi, L., Orgaz, F., García-Tejera, O., Lopez-Bernal, A., González-Dugo, M.V., Ballester-Lurbe, C., Castel, J.R., Alarcón-Cabañero, J.J., Nicolás-Nicolás, E., Girona, J., 2013. Modelling canopy conductance and transpiration of fruit trees in Mediterranean areas: a simplified approach. Agric. For. Meteorol. 171, 93–103.
Vossen, P., 2007. Olive oil: History, production, and characteristics of the world's classic oils. Hortscience 42 (5), 1093–1100.
Xiloyannis, C., Dichio, B., Nuzzo, V., Celano, G., 1999. Defense strategies of olive against water stress. Acta Hortic. 474, 423–426.
Zhang, Y., Xu, M., Chen, H., Adams, J., 2008. Global pattern of NPP to GPP ratio derived from MODIS data: effects of ecosystem type, geographical location and climate. Glob. Ecol. Biogeogr. 18, 280–290.
Zarco-Tejada, P.J., Diaz-Varela, R., Angileri, V., Loudjani, P., 2014. Tree height quantification using very high-resolution imagery acquired from an unmanned aerial vehicle (UAV) and automatic 3D photo-reconstruction methods. Eur. J. Agron. 55, 89–99.